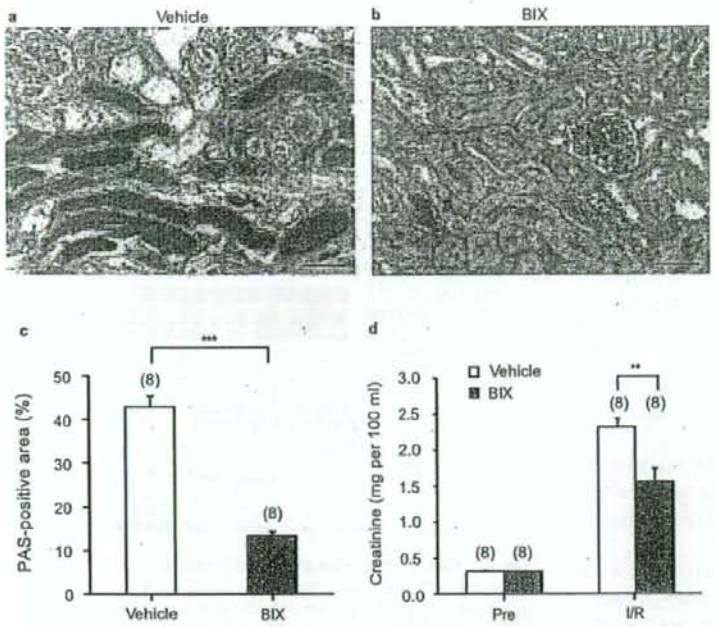

Fig. 2. Effect of BIX on renal I/R injury. Vehicle or BIX was administered to mice 24 h before I/R operation. a, b, c: PAS staining was performed on kidney sections obtained 24 h after I/R from mice treated with vehicle (a) or BIX (b). The cortex is mainly shown. Bars = 50 μm. The PAS-positive area was measured as described previously (8) (c). Values are each a mean ± S.E.M. Numbers in parentheses are the numbers of animals tested. ***P<0.001 *vs* vehicle (Student's t-test). d: Plasma creatinine concentrations before (Pre) and 24 h after I/R are shown. Values are each a mean ± S.E.M. Numbers in parentheses are the numbers of animals tested. **P<0.01 *vs* vehicle (Student's t-test).

tunicamycin (Fig. 1b). BIX and tunicamycin had no effect on the expression level of HSP70, indicating that both agents specifically activated the UPR pathway.

Mice were treated with vehicle or BIX for 24 h and then subjected to renal I/R. At 24 h after renal I/R, renal function and histology with PAS staining were evaluated (Fig. 2). Histological analysis revealed that renal I/R in the vehicle group caused cast formation in tubules, tubular dilatation, and necrosis in the cortex and the outer medulla (Fig. 2a), which was less pronounced in mice treated with BIX (Fig. 2b). The PAS-positive area in the BIX group was significantly smaller than that in the vehicle mice (Fig. 2c). In accordance with the histological results, the plasma concentration of creatinine in the BIX group was significantly lower than that in the vehicle group at 24 h after I/R (Fig. 2d).

Tunicamycin has been shown to be protective against renal I/R injury, accompanied by enhancement of the renal BiP protein level (8). Therefore we compared the expression level of BiP in the kidney following renal I/R between the vehicle and BIX groups. The level of BiP protein was clearly higher in the BIX group (Fig. 3a). In contrast, the level of HSP70 expression did not differ between the groups. These data clearly show that treatment of mice with BIX attenuated renal I/R injury with concomitant enhancement of renal BiP expression, which is similar to the effect of tunicamycin on renal I/R injury.

In order to examine whether the effect of BIX resulted from the activation of the UPR pathway, we compared the effect of treatment with tunicamycin alone with that of a combination of BIX and tunicamycin on I/R-induced renal dysfunction. To this end, we used a dose of tunicamycin, which was known both to efficiently activate the unfolded protein response in the kidney and to exert protection against renal I/R injury (8, 12). As shown in Fig. 3b, no significant additive effect of co-administration was observed, indicating that the two drugs share the same pathway.

Several in vitro and in vivo studies have examined UPR activation in response to renal I/R and its role in preventing cell injury using chemical UPR inducers such as tunicamycin and thapsigargin (6 – 8). However, since these drugs cause the unfolded proteins to accumulate in the ER (1 – 3), their application for therapeutic purposes is unlikely to be realized (9). In order to circumvent this problem, we have searched for a chemical compound that induces BiP through a selective pathway without accumulation of the unfolded proteins and has low cell toxicity; and we finally found BIX, which up-regulates BiP with lower expression of genes mediated by non-ATF6 pathways in the cultured cells and the brain (9, 10). In this study, we examined whether BIX ameliorated renal I/R injury through activation of the UPR via the ATF6 pathway. BIX significantly lessened the severity of renal I/R injury without expression of genes

MOLECULAR AND CELLULAR BIOLOGY, Jan. 2008, p. 165–176 Vol. 28, No. 1
0270-7306/08/$08.00+0 doi:10.1128/MCB.00863-07

Regulation of Notch Signaling by Dynamic Changes in the Precision of S3 Cleavage of Notch-1▽†

Shinji Tagami,[1]‡ Masayasu Okochi,[1]*‡ Kanta Yanagida,[1] Akiko Ikuta,[1] Akio Fukumori,[1] Naohiko Matsumoto,[1] Yoshiko Ishizuka-Katsura,[1] Taisuke Nakayama,[1] Naohiro Itoh,[1] Jingwei Jiang,[1] Kouhei Nishitomi,[1] Kouzin Kamino,[1] Takashi Morihara,[1] Ryota Hashimoto,[1] Toshihisa Tanaka,[1] Takashi Kudo,[1] Shigeru Chiba,[2] and Masatoshi Takeda[1]

Department of Post-Genomics and Diseases, Division of Psychiatry and Behavioral Proteomics, Osaka University Graduate School of Medicine, Osaka 565-0871, Japan,[1] and Department of Cell Therapy and Transplantation Medicine, University of Tokyo Hospital, Bunkyo-ku, Tokyo 113-8655, Japan[2]

Received 16 May 2007/Returned for modification 19 July 2007/Accepted 11 October 2007

Intramembrane proteolysis by presenilin-dependent γ-secretase produces the Notch intracellular cytoplasmic domain (NCID) and Alzheimer disease-associated amyloid-β. Here, we show that upon Notch signaling the intracellular domain of Notch-1 is cleaved into two distinct types of NICD species due to diversity in the site of S3 cleavage. Consistent with the N-end rule, the S3-V cleavage produces stable NICD with Val at the N terminus, whereas the S3-S/S3-L cleavage generates unstable NICD with Ser/Leu at the N terminus. Moreover, intracellular Notch signal transmission with unstable NICDs is much weaker than that with stable NICD. Importantly, the extent of endocytosis in target cells affects the relative production ratio of the two types of NICD, which changes in parallel with Notch signaling. Surprisingly, substantial amounts of unstable NICD species are generated from the Val→Gly and the Lys→Arg mutants, which have been reported to decrease S3 cleavage efficiency in cultured cells. Thus, we suggest that the existence of two distinct types of NICD points to a novel aspect of the intracellular signaling and that changes in the precision of S3 cleavage play an important role in the process of conversion from extracellular to intracellular Notch signaling.

Presenilin (PS)-dependent γ-secretase (PS/γ-secretase) mediates the degradation of transmembrane domains (TMs) in many type 1 receptors, including Notch and β-amyloid protein precursor (βAPP) (18, 52). Degradation of these receptors is characterized by sequential endoproteolysis: following shedding by cleavage in the extracellular juxtamembrane region, the receptors undergo PS-dependent intramembrane proteolysis, releasing amyloid-β (Aβ)-like peptides and intracellular cytoplasmic domains (ICDs) (5, 14). At least in the cases of βAPP, Notch, and CD44, cleavages of the C termini of Aβ-like peptides and of the N termini of ICDs in the TM are distinct. This process of cleavage at two sites is known as "dual cleavage" (33). The process of Aβ generation has been intensively studied, and it is suggested that Aβ is released by a series of sequential cleavages followed by the ICD generation (25, 36, 53). An unusual characteristic of this intramembrane proteolysis is that some of the cleavage sites can vary (42). The precision of cleavage can therefore be defined as the ratio of the cleavage at each site. For example, PS-dependent cleavage of βAPP at the γ site, which is associated with Alzheimer disease (AD), occurs mainly at residue 40 (γ40), producing Aβ40, and at residue 42 (γ42), producing Aβ42. A small increase in the proportion of γ42 to γ40 cleavage is consistently observed in many familial AD (FAD)-associated PS or βAPP mutants (42), but it is unclear whether such changes in the precision of PS-dependent intramembrane proteolysis have any biological effects.

Notch signaling, which is essential for development, is a type of local-cell signaling that participates in neurodegeneration and tumorigenesis (1). The canonical Notch pathway is mediated by the regulated intramembrane proteolysis pathway, in which Notch receptors undergo ligand-dependent sequential endoproteolysis via a series of enzymes, including PS/γ-secretase (8). The Notch-1 ICD (NICD), which is produced by PS/γ-secretase-mediated cleavage at site 3 (S3), translocates to the nucleus and participates in transactivation of target genes (40). Elimination of PS function results in the Notch phenotype, which includes disruption of segmentation during the development of many kinds of animals, demonstrating the importance of NICD generation (41).

The intensity of Notch signaling is crucial for cell fate decisions. For example, Notch haplo-insufficiency causes the "notched-wing" phenotype in *Drosophila* (9). Reduced Notch activity favors the γδ T-cell fate over the αβ T-cell fate, whereas a constitutively activated form of Notch produces a reciprocal phenotype (48). The endocytosis of Notch and its ligands plays a key role in the regulation of the signaling intensity (40), but the biochemical aspects regulating this process have not been well studied. N-terminal amino acid se-

* Corresponding author. Mailing address: Department of Post-Genomics and Diseases, Division of Psychiatry and Behavioral Proteomics, Osaka University Graduate School of Medicine, D3, Yamada-oka 2-2, Suita, Osaka 565-0871, Japan. Phone: 81-6-6879-3053. Fax: 81-6-6879-3059. E-mail: mokochi@psy.med.osaka-u.ac.jp.

† Supplemental material for this article may be found at http://mcb.asm.org/.

‡ These authors contributed equally to this work.

▽ Published ahead of print on 29 October 2007.

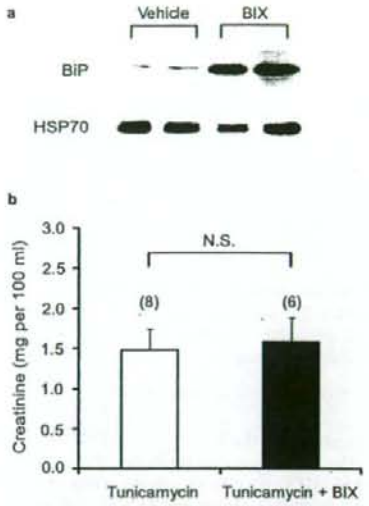

Fig. 3. Effect of BIX on renal BiP expression after renal I/R and effect of co-administration of tunicamycin on BIX-induced renal protection. a: Representative immunoblots for BiP and HSP70. Vehicle or BIX was administered to mice at 24 h before I/R operation, and kidneys were removed 24 h after I/R. Protein was extracted from whole kidney. b: Mice were treated with tunicamycin for 24 h and then were treated with vehicle or BIX for another 24 h. Thereafter, mice were subjected to I/R operation. Plasma creatinine concentrations at 24 h after I/R are shown. Values are each a mean ± S.E.M. N.S., not significant. Numbers in parentheses are the numbers of animals tested. It was noteworthy that the creatinine concentration in the co-administration group (tunicamycin + BIX) was similar to that in the group treated with BIX alone (Fig. 2d).

mediated by non-ATF6 pathways. Furthermore, tunicamycin co-administration provided no additional protective effect. Our data strongly suggest that BIX exerts its protective effect through activation of the UPR via the ATF6 pathway and that BIX may be a potential therapeutic agent for ischemic AKI caused by renal I/R.

Acknowledgment

This work was supported in part by JSPS KAKENHI, 19580342 (M.I.).

References

1 Schröder M, Kaufman RJ. The mammalian unfolded protein response. Annu Rev Biochem. 2005;74:739–789.
2 Feldman DE, Chauhan V, Koong AC. The unfolded protein response: a novel component of the hypoxic stress response in tumors. Mol Cancer Res. 2005;3:597–605.
3 Yoshida H. ER stress and diseases. FEBS J. 2007;274:630–658.
4 Devarajan P. Update on mechanisms of ischemic acute kidney injury. J Am Soc Nephrol. 2006;17:1503–1520.
5 Ikeda M, Prachasilchai W, Burne-Taney MJ, Rabb H, Yokota-Ikeda N. Ischemic acute tubular necrosis models and drug discovery: a focus on cellular inflammation. Drug Discov Today. 2006;11:364–370.
6 Bush KT, George SK, Zhang PL, Nigam SK. Pretreatment with inducers of ER molecular chaperones protects epithelial cells subjected to ATP depletion. Am J Physiol Renal Physiol. 1999;277:F211–F218.
7 George SK, Meyer TN, Abdeen O, Bush KT, Nigam SK. Tunicamycin preserves intercellular junctions, cytoarchitecture, and cell-substratum interactions in ATP-depleted epithelial cells. Biochem Biophys Res Commun. 2004;322:223–231.
8 Prachasilchai W, Sonoda H, Yokota-Ikeda N, Oshikawa S, Aikawa C, Uchida K, et al. A protective role of unfolded protein response in mouse ischemic acute kidney injury. Eur J Pharmacol. 2008;592:138–145.
9 Kudo T, Kanemoto S, Hara H, Morimoto N, Morihara T, Kimura R, et al. A molecular chaperone inducer protects neurons from ER stress. Cell Death Differ. 2008;15:364–375.
10 Oida Y, Izuta H, Oyagi A, Shimazawa M, Kudo T, Imaizumi K, et al. Induction of BiP, an ER-resident protein, prevents the neuronal death induced by transient forebrain ischemia in gerbil. Brain Res. 2008;1208:217–224.
11 Sharyo S, Yokota-Ikeda N, Mori M, Kumagai K, Uchida K, Ito K, et al. Pravastatin improves renal ischemia-reperfusion injury by inhibiting the mevalonate pathway. Kidney Int. 2008;74:577–584.
12 Kondoh M, Tsukada M, Kuronaga M, Higashimoto M, Takiguchi M, Himeno S, et al. Induction of hepatic metallothionein synthesis by endoplasmic reticulum stress in mice. Toxicol Lett. 2004;148:133–139.

quencing revealed that S3 in mouse Notch-1 lies between Gly1743 and Val1744 (murine Notch-1 numbering) (39). Whether the site of S3 cleavage can vary has not been examined previously.

In this study, we found that there is diversity in the site of S3 cleavage, resulting in the production of two types of NICD with apparently distinct stability and ability to transmit Notch signaling in cultured cells. Our results suggest that the precision of PS/γ-secretase-mediated cleavage is important for determining the intensity of Notch signaling.

MATERIALS AND METHODS

Antibodies. To generate affinity-purified polyclonal N-terminal capping antibodies to NICD-S (anti-NT-S), rabbits were immunized with a synthetic peptide (SRKRR) corresponding to the N terminus of NICD-S(+3). We also prepared two kinds of affinity columns in which the N-terminal peptide of NICD-V (VLLSRKRR) or NICD-S (SRKRR) was conjugated to Sepharose 4B (Amersham). We isolated the fraction of the anti-NT-S antiserum that bound to the NICD-S(+3) column but not the NICD-V column (32). Anti-NT-L antiserum was raised against a synthetic peptide (LLSRKRR) corresponding to the N terminus of NICD-L(+1) and then purified by affinity chromatography on Sepharose 4B conjugated to the N-terminal peptide of NICD-L (LLSRKRR), followed by a second step of affinity chromatography on Sepharose 4B conjugated to the NICD-S peptide (SRKRR). Other antibodies were purchased from commercial sources as follows: anti-NT-V (V1744 antibody) from Cell Signaling; antinicastrin and antibody mN1A against Notch-1 from Sigma-Aldrich; antibody H114 against Jagged-1 and antitubulin from Santa Cruz Biotechnology; anti-early endosome antigen 1 and anti-GM130 from BD Transduction Laboratories; antibody 12CA5 against the HA epitope from Roche Diagnostics, Inc.; antibody 9E10 against the myc epitope from Zymed; and anti-Na-K ATPase from Upstate Biotechnology.

cDNA constructs. The cDNA encoding the mouse Notch-1 variant NEXT was previously described (33). NEXTΔC was generated by PCR-based mutagenesis using the QuikChange-II kit (Stratagene) with NEXT cDNA as a template. The mutant versions of NEXT and NEXTΔC were generated using the same kit. To generate expression constructs for polypeptides NICD-V, NICD-L (+1), and NICD-S (+3), cDNAs encoding Val, Leu(+1), and Ser(+3) as the N termini were subcloned into the pASK-IBA6 vector (IBA). *HES-1*-luc (a kind gift from Alain Israel) (16) and pGa981-6 (a kind gift from Georg W. Bornkamm) (21) were used as described. For more sensitive detection of *HES-1* promoter transactivation, we newly generated a *hairy and enhancer of split-Y* (*HES-Y*) construct containing four sequential RBP-Jκ binding sites in the *HES-1* promoter region.

Cell culture. We generated HEK293 cells expressing PS1 R278I (a kind gift from M. Nishimura) (27) or PS1 G384A (a kind gift from H. Steiner) (44). HEK293 cells expressing either wild-type (wt) or mutants of PS1 were previously described (31). These cells were transfected with wt, mutant NEXT, or mutant NEXTΔC. HeLa cells expressing Dyn-1 K44A (a kind gift from S. Schmid) were used as described and stably transfected with NEXT or NEXTΔC. CHO(r) cells (a gift from S. Shirahata) (29) were stably transfected with mouse Notch-1 or Jagged-1.

Cell-free Notch-1 cleavage assay. To obtain crude membrane fractions (CMFs), cells were homogenized in buffer (0.25 M sucrose and 10 mM HEPES, pH 7.4) containing a protease inhibitor cocktail (Roche), followed by centrifugation at 1,000 × *g* for 5 min. The postnuclear supernatant was further centrifuged at 100,000 × *g* for 30 min, and the resulting pellet was collected. This CMF was resuspended in 150 mM sodium citrate buffer (pH 6.4) containing a 4× concentration of protease inhibitor cocktail (Sigma-Aldrich) and 5 mM 1,10-phenanthroline (Sigma-Aldrich), incubated for 20 min at 37°C, and then centrifuged at 100,000 × *g* for 30 min (11).

Pulse-chase experiments. Pulse-chase experiments were performed as described previously (11, 30, 31, 33, 34).

Immunoprecipitation/MALDI-TOF MS. Immunoprecipitation and matrix-assisted laser desorption ionization–time-of-flight mass spectrometry (MALDI-TOF MS) analysis was carried out as described previously (11, 31, 33). The heights of the MS peaks and molecular weights were calibrated using angiotensin and bovine insulin β-chain as standards (Sigma-Aldrich).

Immunoprecipitation-immunoblotting and immunoprecipitation-autoradiography. Metabolically labeled or unlabeled lysates were lysed in radioimmunoprecipitation assay buffer (1% Triton X-100, 0.5% sodium deoxycholate, and 0.1% sodium dodecyl sulfate [SDS]) containing a protease inhibitor mix (Sigma-Aldrich). The cell lysates were centrifuged at 10,000 × *g* for 15 min, and the supernatant fractions were immunoprecipitated as indicated. Following 8% Tris-glycine (Tefco) or 10 to 20% Tris-Tricine (Invitrogen) SDS-polyacrylamide gel electrophoresis (SDS-PAGE), the gels were either transferred to a polyvinylidene difluoride membrane and probed with the indicated antibodies or dried and analyzed by autoradiography. To quantitatively measure the levels of NICD species in cultured cells, several doses of each NICD polypeptide were separated together with samples by SDS-PAGE and analyzed by immunoblotting with the corresponding N-terminal capping antibody. The chemiluminescence intensities were measured using an LAS3000 scanner, followed by analysis with Multi Gauge Ver3.0 software (Fuji Film). Biotinylated transferrin was semiquantitatively measured by chemiluminescence using the scanner, followed by analysis with the software.

Cell-cell association assay. For the detection of de novo NICD species, CHO(r) cells stably expressing Notch-1 were grown to confluence in 150-mm dishes (2×10^7 cells per dish) in triplicate. Next, 3×10^7 CHO(r) cells stably expressing Jagged-1 were spread over the Notch-1-expressing cells. After 8 h of coculture, the cells were collected. For the reporter assay, the procedure was the same, although it was carried out in a 12-well plate and the number of cells was reduced accordingly.

cDNA transfection and reporter assay. To examine the intensity of Notch signaling, we used a dual luciferase reporter assay system (Promega) as described by the manufacturer (31). Briefly, cells expressing Notch-1 or its derivatives in a 12-well plate were transiently transfected with 125 ng of *HES-Y* or pGa981-6 and 1.25 ng of the control *Renilla* luciferase reporter plasmid pRL-TK. The reporter assay was performed on the next day. Dyn-1 K44A expression was induced with various concentrations of tetracycline 24 h prior to transfection with *HES-Y*. Cell-cell association was performed 24 h after transfection with *HES-Y*.

Preparation of nuclear extract from mouse tissues. A nuclear complex co-IP kit (Active Motif) was used to obtain nuclear extracts from C57BL/6 (Japan SLC) mouse tissues. Homogenized adult mouse brain or fetal mouse tissues without internal organs (embryonic day 12) were treated according to the manufacturer's instructions. Subsequently, the nuclear extracts were diluted using the immunoprecipitation buffer included in the kit, precleared three times with protein G- or protein A-Sepharose, and immunoprecipitated according to the manufacturer's instructions.

Purification of polypeptides. NICD-V, NICD-L(+1), and NICD-S(+3) polypeptides fused with *strept*-tag-II followed by an N-terminal factor Xa cleavage site were obtained by transforming *Escherichia coli* (BL21) with pASK-IBA6 (IBA) encoding each polypeptide. Briefly, after the expression was induced, the cells were collected by centrifugation at 4,500 × *g* for 12 min, resuspended in ice-cold TSE buffer (10 mM Tris-HCl [pH 7.4], 20% sucrose, and 2.5 mM Na-EDTA), and then incubated on ice for 10 min. The cells were again collected by centrifugation, resuspended in ice-cold water, incubated for 10 min, briefly sonicated, and sedimented by centrifugation at 14,000 × *g* for 15 min (osmotic shock fractionation). The supernatant was passed through a Strep-Tactin Sepharose column (IBA). Bound polypeptides were eluted with phosphate-buffered saline containing 2.5 mM desthiobiotin. Eluted polypeptides were treated with factor Xa (Sigma-Aldrich), and the solution was passed through the column again to remove uncleaved polypeptide (34). The purity of the polypeptides was confirmed by 6% Tris-glycine SDS-PAGE, followed by staining with Coomassie brilliant blue.

Loading of polypeptides. The polypeptides obtained as described above were loaded into cells using Chariot protein transfection reagent (Active Motif) according to the manufacturer's instructions. Briefly, cells were grown and transfected with reporter genes in a 12-well plate. The cells were then loaded with 5 μg of each polypeptide or bovine serum albumin (BSA) along with 0.5 μg of β-galactosidase, using 15 μl of Chariot reagent per well. Finally, the cells were stained for β-galactosidase or used for the reporter assay.

In vitro degradation assay. NICD polypeptides (0.2 μg) were mixed with 60 μl of fresh rabbit reticulocyte lysate (Promega) and incubated at 37°C. Clasto-lactacystin (10 μM), MG262 (100 nM), and 4-hydroxy-5-iodo-3-nitrophenyl-acetyl-Leu-Leu-leucinal-vinyl sulfone (NLVS) (10 μM) were added to inhibit the action of the proteasome.

Transferrin uptake assay. To estimate the rate of endocytosis, the levels of internalized and surface-bound biotinylated-transferrin were measured as described previously (11).

Subcellular fractionation. Linear gradients of 2.5% to 25% iodixanol (Optiprep; Axis-Shield) were prepared, and fractionation was performed as previously described (11).

Statistical analysis. Experiments were performed at least three times unless otherwise indicated. Representative results are shown for cell-free immunoprecipitation/MALDI-TOF MS, immunoblotting, immunoprecipitation-autoradiog-

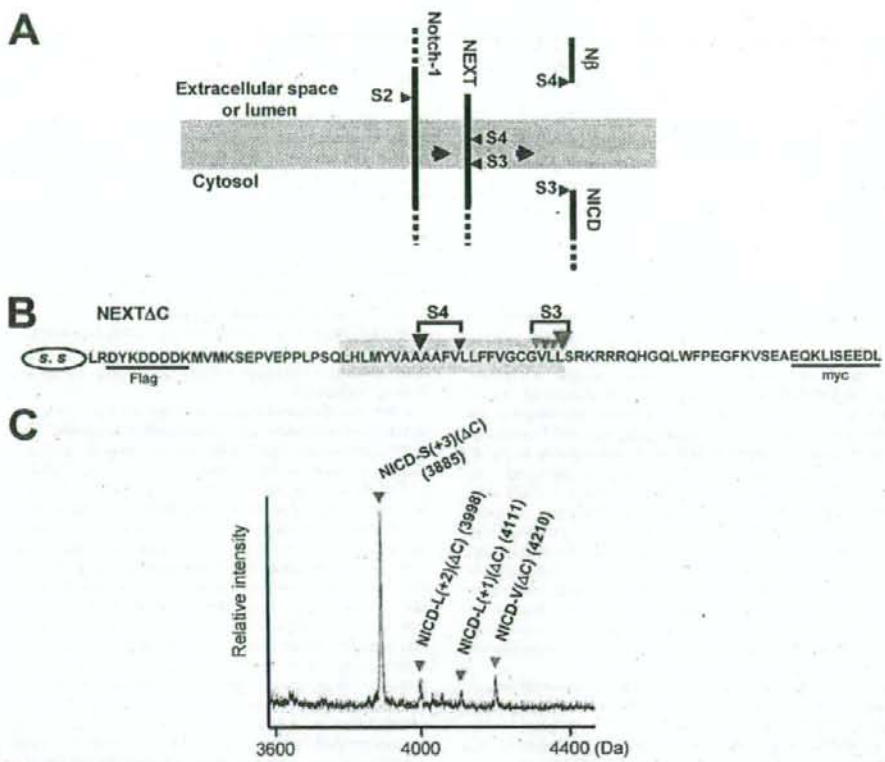

FIG. 1. MALDI-TOF MS analysis of NICD(ΔC) produced by the cell-free Notch-1 cleavage assay. (A) Schematic representation of sequential endoproteolysis of Notch-1. S2 to S4 and the gray area represent the proteolytic sites and the putative TM, respectively. (B) Schematic representation of the NEXTΔC construct used in the cell-free Notch-1 cleavage assay. Colored inverted triangles show the S3 and S4 proteolytic sites. SS, signal sequence. (C) MS spectrum of de novo NICD(ΔC) generated in the cell-free assay. CMF was derived from K293 cells stably expressing NEXTΔC. The molecular mass of each species is indicated. To inhibit degradation by proteases other than aspartyl proteases, BSA and a mixture of metallo-, serine, and cysteine protease inhibitors were added to the cell-free assay buffer. Colored inverted triangles indicate the NICD(ΔC) species produced by cleavage at the sites shown in panel B.

raphy, and immunocytochemistry. The statistical significance of differences was determined by Student's *t* test.

RESULTS

A cell-free Notch-1 cleavage assay indicates diversity in the site of S3 cleavage. The cleavage of the Notch-1 TM occurs at least at two sites, one at S3, which determines the N terminus of intracellularly liberated NICD (39), and the other at S4, which determines the C terminus of extracellularly secreted Nβ (Fig. 1A) (31, 33). We first examined the diversity of the S3 cleavage site. We constructed NEXTΔC, a mouse Notch-1 derivative that lacks the majority of its extracellular and intracellular domains (Fig. 1B), and we established a cell-free Notch-1 cleavage assay using the CMF from cells stably expressing this construct (11). The de novo-generated NICD(ΔC) was immunoprecipitated with anti-myc antibodies and then analyzed by MALDI-TOF MS (Fig. 1C). Strikingly, proteolysis at S3 did not occur at a unique site but rather occurred at multiple sites, as indicated by the presence of multiple sizes of NICD(ΔC) (see Table S1 in the supplemental material). Specifically, proteolysis at S3 occurred at the following sites: S3-L(+1), between Val1744 and Leu1745; S3-L(+2), between Leu1745 and Leu1746; S3-S(+3), between Leu1746 and Ser1747; and the previously reported S3-V, between Gly1743 and Val1744 (39) (Fig. 1B; see Fig. S1A in the supplemental material). Unexpectedly, the highest peak was for NICD-S(+3)(ΔC) rather than NICD-V(ΔC) (Fig. 1C), suggesting that S3-S(+3) is the major site of S3 cleavage under these assay conditions. Addition of the PS/γ-secretase inhibitors eliminated the cleavage at both S3-V and S3-S(+3) (see Fig. S1B in the supplemental material). Moreover, we did not observe generation of these shorter NICD(ΔC) species from the longer NICD(ΔC) (see Fig. S1C in the supplemental material). Therefore, the results are consistent with the possibility that all the fragments are produced by PS-dependent S3 cleavage in the Notch-1 TM.

Diversity in the site of S3 cleavage in living cells. To identify the N terminus of NICD molecules in vivo, we prepared two N-terminal capping antibodies, anti-NT-V (anti-V1744) and anti-NT-S (32), and corresponding recombinant NICD species

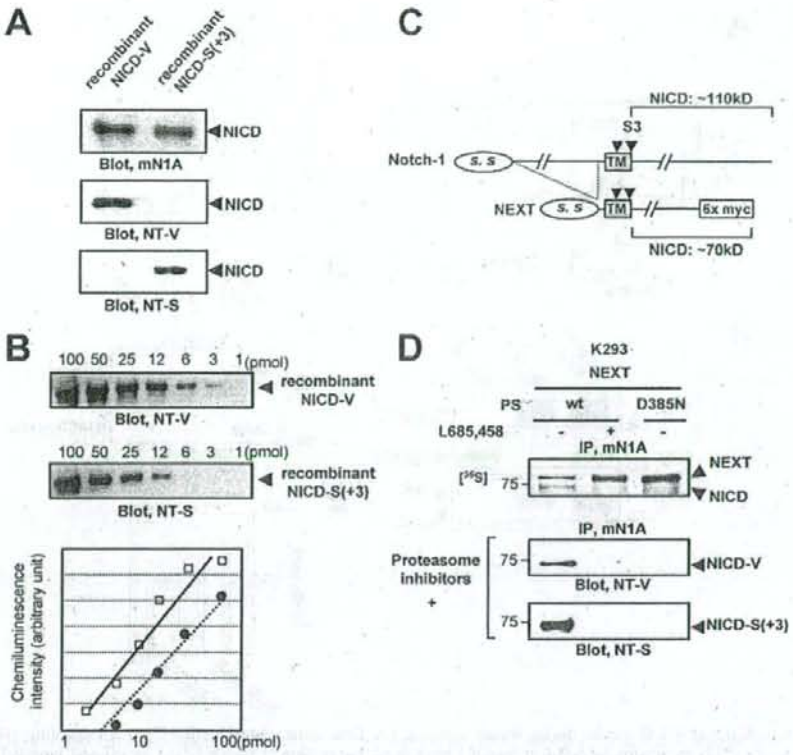

FIG. 2. Characterization of capping antibodies to the N terminus of NICD and detection of distinct NICD species in cultured cells. (A) Specificities of the anti-NT-V and the anti-NT-S antibodies. Immunoblotting with antibody mN1A confirmed that equal amounts of the polypeptides were loaded in each lane (upper panel). (B) Affinities of the anti-NT-V and anti-NT-S antibodies. The indicated amounts of NICD-V or NICD-S(+3) were separated by SDS-PAGE and analyzed by immunoblotting with the anti-NT-V or anti-NT-S antibody, respectively. The graph shows the chemiluminescence intensity versus the concentration of NICD-V (squares) or NICD-S(+3) (circles). Each antibody detected the respective polypeptide in a dose-dependent manner. (C) Schematic representation of Notch-1 and NEXT constructs. The C-terminal portion of the NEXT construct is replaced by myc_6, while full-length Notch-1 has no modification. Note that the molecular mass of NICD generated from NEXT-myc_6 is ~70 kDa, while that of NICD generated from unmodified Notch-1 is ~110 kDa. (D) Generation of NICD-V and NICD-S(+3) in cultured cells. Proteasome inhibitors lactacystin (10 μM), MG262 (100 nM), and NLVS (10 μM) were added to the medium 12 h prior to cell collection.

with distinct N termini (Fig. 2A; see Fig. S2A in the supplemental material). We found that (i) the anti-NT-V antibody specifically recognizes recombinant NICD-V but not NICD-S(+3) (34) (Fig. 2A, middle panel; see Fig. S2B in the supplemental material), whereas the anti-NT-S antibody has the opposite specificity (Fig. 2A; lower panel, see also Fig. S2B in the supplemental material), and (ii) these antibodies can be used to determine the relative amounts of NICD-V and NICD-S(+3) generated, that is, the extents of S3-V and S3-S(+3) cleavage, respectively (Fig. 2B).

Using these capping antibodies, we examined the diversity in the site of S3 cleavage in living cells. The Notch extracellular truncation (NEXT) (Fig. 2C), which lacks the majority of the extracellular domain of Notch-1, undergoes constitutive ligand-independent intramembrane proteolysis by PS/γ-secretase (24). We prepared cells stably expressing NEXT and wt or a dominant-negative form of PS1 (PS1 D385N) (51). A 30-min pulse with [^{35}S]methionine followed by a 2-h chase revealed production of an ~70-kDa NICD band that completely disappeared upon elimination of PS/γ-secretase function (Fig. 2D, upper panel). Because degradation of NICD is mediated by the ubiquitin-proteasome pathway (8, 40, 41), we added a potent proteasome inhibitor mixture consisting of lactacystin, MG262, and NLVS (Fig. 2D, middle and lower panels). The resulting cell lysates were immunoprecipitated with antibody mN1A, separated by SDS-PAGE, and analyzed by immunoblotting with anti-NT-V or anti-NT-S. The anti-NT-V and anti-NT-S antibodies specifically detected the PS-dependent production of NICD-V and NICD-S(+3), respectively (Fig. 2D, middle and lower panels; see Fig. S2C in the supplemental material). We also confirmed that both NICD-V and NICD-S(+3) are produced in cells in the absence of the proteasome inhibitor mixture (see Fig. S2D in the supplemental material).

S3 cleavage during Notch signaling produces distinct molecular species of NICD. Because ligand-induced degradation of Notch receptors is initiated at the plasma membrane (PM),

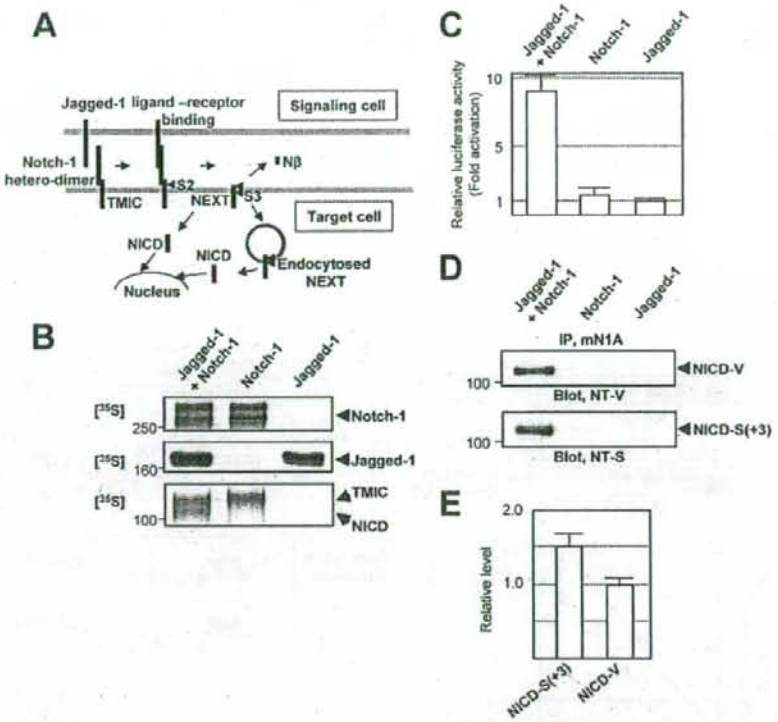

FIG. 3. Detection of different NICD species during Notch signaling. (A) Schematic representation of Notch signaling. (B) Notch signaling in cell culture. CHO(r) cells stably expressing Jagged-1 or Notch-1 were used. Expression of Notch-1 (top panel) and Jagged-1 (middle panel) was determined by a 1-h pulse experiment, followed by immunoprecipitation using antibodies mN1A and H114, respectively. The precipitated proteins were analyzed by SDS-PAGE, followed by autoradiography. A 1-h pulse/2-h chase experiment detected an ~110-kDa NICD band only when the cells were cocultured (bottom panel). (C) Notch signaling was measured using a dual luciferase assay. The relative luciferase activity of Jagged-expressing cells was defined as 1.0. Values represent means ± standard deviations (n = 3). (D) In the presence of the proteasome inhibitors, both NICD-V (upper panel) and NICD-S(+3) (lower panel) were detected during Notch signaling. The bands were detected as described for Fig. 2D. (E) Relative levels of NICD-S(+3) and NICD-V generated during Notch signaling. The relative levels were calculated based on the standard curve shown in Fig. 2B.

intramembrane proteolysis of Notch-1 is thought to occur at restricted subcellular locations, such as the PM and endocytosed vesicles (13, 17, 20) (Fig. 3A). We prepared cells stably expressing either Jagged-1 (a Notch ligand) or full-length Notch-1 and then cocultured them. We determined the extent of Notch signaling using a luciferase reporter assay in cells expressing a newly improved construct, *HES-Y* (see Materials and Methods for details). Pulse-chase experiments revealed that upon coculture, sequential endoproteolysis of Notch-1 occurs, producing the NICD band (Fig. 3B, bottom panel). Moreover, when the cells were cocultured, we observed concomitant activation of the *HES-1* promoter (Fig. 3C). The results therefore demonstrate Notch-1 signaling in cell culture. Using this assay system, we investigated whether NICD-S(+3) and NICD-V are indeed generated during Notch signaling. Strikingly, upon coculture, both NICD-V and NICD-S(+3) were detected (Fig. 3D, upper and lower panels). The intensities of the bands indicated that 1.5-fold more NICD-S(+3) than NICD-V was produced (Fig. 3E). Therefore, the results indicated that there are multiple forms of NICD produced during Notch signaling.

We next tried to detect the NICD-V and NICD-S(+3) in fetal (embryonic day 12, whole embryo without internal organs) and adult (brain) mouse tissues (Fig. 4). Nuclear extracts from these tissues were immunoprecipitated with mN1A, which specifically recognizes intracellular domain of Notch-1 but not Notch-2, -3, or -4. The precipitated proteins were then analyzed by SDS-PAGE, followed by immunoblotting with anti-NT-V or anti-NT-S antibodies. As shown in Fig. 4A, we clearly found both NICD-V (upper panel) and NICD-S(+3) species (lower panel) in the fetal mouse tissues, but these species were barely detectable in adult brains. This is consistent with the finding of a high level of Notch signaling in fetal mouse tissue (22). Moreover, we successfully detected the same NICD-V and NICD-S bands in the mouse embryo even when the combination of antibodies used for immunoprecipitation and immunoblotting was swapped (Fig. 4B). Therefore, the results indicated that multiple forms of NICD are produced in vivo.

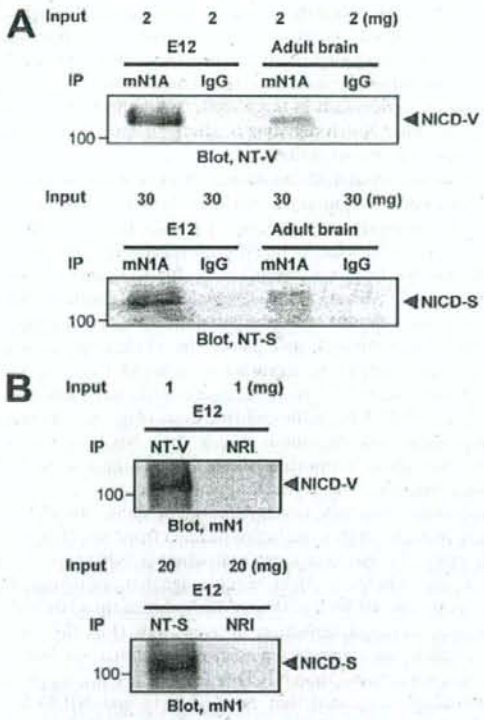

FIG. 4. Detection of NICD-V and NICD-S(+3) in vivo. The indicated amounts of nuclear extracts were loaded for immunoprecipitation. IgG and NRI, isotype-matched immunoglobulin and normal rabbit immunoglobulin, respectively.

Transactivation of the HES-1 promoter by NICD-S(+3) is much weaker than transactivation by NICD-V in living cells. The stability of polypeptides degraded by the ubiquitin-proteasome pathway depends on the N-end rule, where an N-terminal valine is a stabilizing residue and an N-terminal serine is destabilizing (2, 12). Therefore, we examined whether the intensity of Notch signaling differs for NICD-V and NICD-S(+3) in living cells. We loaded *HES-Y*-transfected cells with equal amounts of purified NICD-V or NICD-S(+3) (see Fig. S3 in the supplemental material). After a 1-h loading period, the cells contained similar levels of each NICD species (Fig. 5A). Induction of Notch signaling by chasing the loaded cells for 4 h (signaling period) resulted in much less luciferase activity in the NICD-S-loaded cells than in NICD-V-loaded cells, demonstrating that NICD-S(+3) is much weaker than NICD-V at activating the promoter in living cells (Fig. 5B, left panel).

We next investigated whether the rates of degradation by the proteasome pathway differ for the various species of NICD in an in vitro assay. We incubated recombinant NICD-V or NICD-S(+3) (34) with rabbit reticulocyte lysate (Promega) (12) and examined the levels of the two types of NICD by immunoblotting (Fig. 5C). Our results indicated that NICD-S(+3) is much less stable than NICD-V (Fig. 5D). Moreover, following the proteasome inhibitor treatment, the relative luciferase activities in NICD-S- and NICD-V-loaded cells turned out to be almost the same (Fig. 5E). Collectively the results suggest that unstable NICD-S(+3) may have a much weaker ability than stable NICD-V to mediate intracellular signaling.

The precision of S3 cleavage is distinct in the subcellular locations where it occurs. A previous study showed that the precision of ε cleavage of βAPP, which topologically corresponds to S3 cleavage of Notch-1, differs before and after endocytosis (11). To determine whether S3 cleavage precision differs on PM and endosomes, we performed the cell-free assay using organelles separated by iodixanol gradient fractionation from NEXTΔC-expressing HeLa cells (11). Fractions from a 2.5% to 25% linear iodixanol gradient were examined by immunoblotting with antibodies to early endosome antigen 1 (endosome marker), Na-K ATPase (PM marker), GM130 (Golgi marker), or nicastrin (a component of the PS complex) (Fig. 6A). NICD(ΔC) was generated in the cell-free assay using membranes collected by centrifugation from the endosome-rich (fraction 3) and the PM-rich (fraction 7) fractions and analyzed by immunoprecipitation/MALDI-TOF MS. Remarkably, the relative ratio of NICD-V(ΔC) to NICD-S(+3)(ΔC) was much higher in the PM-rich fraction than in the endosome-rich fraction (Fig. 6B). This indicates that cleavage at S3-V, which generates the longer NICD-V(ΔC), and at S3-S(+3), which generates the shorter NICD-S(+3)(ΔC), occurs predominantly on the PM and endosomes, respectively. This is very similar to the case of ε cleavage of βAPP (11). Subsequently, we investigated the effect of endocytosis on the precision of S3 cleavage. To down-regulate endocytosis, we used cells that express a dominant-negative mutant of dynamin-1 (Dyn-1 K44A) upon tetracycline withdrawal (Fig. 6C) or treatment with bafilomycin A1 (11) (see Fig. S4 in the supplemental material). When endocytosis was strongly inhibited, the precision of S3 cleavage changed drastically, so that the S3-V site instead of the S3-S(+3) site became the major site of cleavage in the cell-free assay (Fig. 6C; see Fig. S4A in the supplemental material). These results from the cell-free assay suggest that generation of stable NICD-V and unstable NICD-S occur predominantly on the PM and endosomes, respectively.

The precision of S3 cleavage changes in parallel with the rate of endocytosis in target cells. Next, we investigated whether these phenomena also occur in living cells. We examined the influence of the rate of endocytosis of NEXT by altering the expression of Dyn-1 K44A in living cells (Fig. 7A). Measurement of biotinylated transferrin uptake revealed various rates of endocytosis in Dyn-1 K44A-expressing cells (Fig. 7B). Strikingly, we found that the ratio of S3-V to S3-S(+3) is low in cells with a high rate of endocytosis and, conversely, that the ratio is high in cells with a low rate of endocytosis (Fig. 7C), which is consistent with the result from the cell-free assay (Fig. 6C). We observed a similar change in the S3 cleavage when endocytosis was blocked with bafilomycin A1 (see Fig. S4B in the supplemental material). Therefore, it appears that the precision of S3 cleavage changes in parallel with the rate of endocytosis, and relative generation of stable NICD-V increases as the rate of endocytosis decreases.

Because Notch signaling is associated with endocytosis of Notch receptors and/or Notch ligands during development (3, 28, 35, 40, 43), we next examined the effect of the change in S3

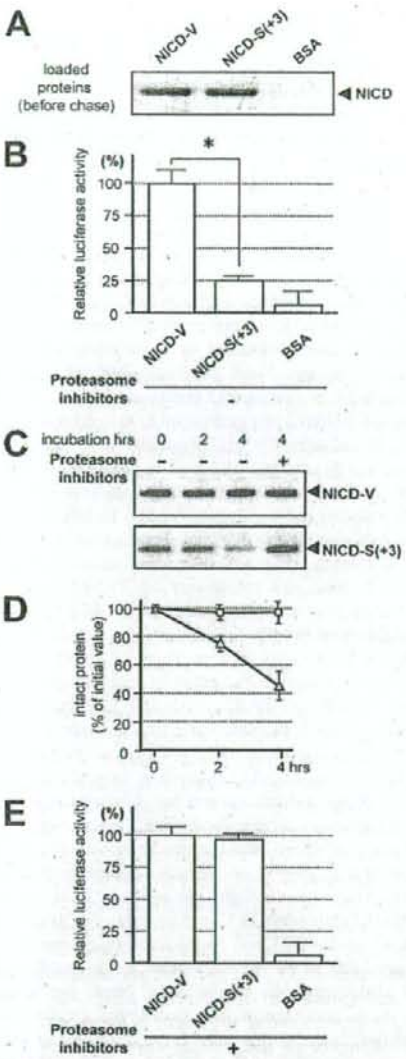

FIG. 5. Characterization of the NICD species. (A) Loading of cells with NICD. HeLa cells (2.5×10^5) were loaded with 5 μg of purified NICD-V, NICD-S(+3), or BSA (control). The cells were collected 1 h after the addition of the Chariot macromolecule complex (defined as the loading period). (B) Assay of Notch downstream signaling induced by the NICD species. The NICD-loaded cells from panel A were chased for 4 h and collected, and Notch downstream signaling was assayed. The values were corrected for background luciferase activity (0.5 μg of β-galactosidase-loaded cells), and the luciferase activity in the NICD-V-loaded cells was defined as 100%. Values represent means ± standard deviations ($n = 3$). The asterisk indicates that the relative luciferase activity in NICD-V-loaded cells is statistically different than that in NICD-S(+3)-loaded cells ($P < 0.001$). Similar results were obtained using cells expressing pGa981-6 (data not shown). (C) Stability of recombinant NICD species in rabbit reticulocyte lysate. Note that the degradation of NICD-S(+3) was inhibited in the presence of proteasome inhibitors. (D) Levels of intact NICDs in the lysates during in vitro degradation. The amount of intact polypeptide was determined using a standard curve of the chemiluminescence intensities of the bands versus their concentrations (data not shown). Squares and triangles indicate the means for NICD-V and NICD-S(+3), respectively. Values represent means ± standard deviations ($n = 3$). (E) Assay of Notch downstream signaling induced by the NICD species in the presence of the proteasome inhibitor mixture. Experiments were performed as described for panel B in the presence of the proteasome inhibitor mixture. The values were corrected for background luciferase activity (0.5 μg of β-galactosidase-loaded cells), and the luciferase activity in the NICD-V-loaded cells was defined as 100%. Values represent means ± standard deviations ($n = 3$).

precision on the intensity of Notch signaling. Surprisingly, we observed a higher intensity of Notch signaling in cells in which the rate of endocytosis of NEXT was lower (Fig. 7D; see Fig. S4C in the supplemental material). These results suggest that the rate of endocytosis in target cells could affect the intensity of intracellular Notch signaling by changing the precision of S3 cleavage and thus its stability.

Mutations around S3 can induce changes in the precision of the cleavage. S3 mutations, such as the Val→Gly mutation (V1744G mutant) and the Lys→Arg mutation (K1749R mutant), cause a decrease in the NICD level (13, 15). To date, this reduction has been considered to be due to decreased NICD generation. However, since we revealed that multiple NICD species with different stabilities are generated, we investigated whether these mutants also change the S3 cleavage precision, which would accelerate degradation of NICD. First, we determined the precision of the S3 cleavage of the Val→Gly mutant version of NEXTΔC in the cell-free assay (Fig. 1C). Strikingly, this mutant was degraded mainly into NICD-L(+1)(ΔC), which has Leu1745 (murine Notch-1 numbering) at its N terminus (Fig. 8A). Therefore, it appears that the Val→Gly mutation causes not only a complete loss of stable NICD-V, but also a dramatic shift in the major product from NICD-S(+3) to NICD-L(+1). We next examined whether NICD-L(+1) behaved like NICD-S(+3) in cellular signal transduction. Like NICD-S(+3), NICD-L(+1) was much weaker than NICD-V at inducing promoter activation in living cells (Fig. 8B). Moreover, our in vitro degradation assay revealed that NICD-L(+1) was much less stable than NICD-V (Fig. 8C). Thus, our in vitro experiments suggested that NICD-L(+1) and NICD-S(+3) are both unstable and have similar effects on Notch signaling but that their effects are distinct from those of NICD-V. We further investigated whether the precision change in the mutant is also observed in living cells. To specifically detect NICD-L(+1), we generated anti-NT-L, an N-terminal capping antibody (see Fig. S5 in the supplemental material). As is clearly shown in Fig. 8D, although almost no NICD-V was detected, a substantial amount of NICD-L(+1) was detected in the Val→Gly version of NEXT-expressing cells. These results indicate that the relative production of unstable NICDs with respect to stable NICD increases in the mutant NEXT cells due to change of the S3 cleavage precision.

The Lys→Arg mutant NEXT (the K1749R mutant) is neither monoubiquitinated nor endocytosed (13). This mutant, like the Val→Gly mutant, causes decreased NICD levels in cell culture (13). Analysis to determine the precision of the S3 cleavage of the Lys→Arg mutant version of NEXTΔC was performed in the cell-free assay. Surprisingly, the Lys→Arg

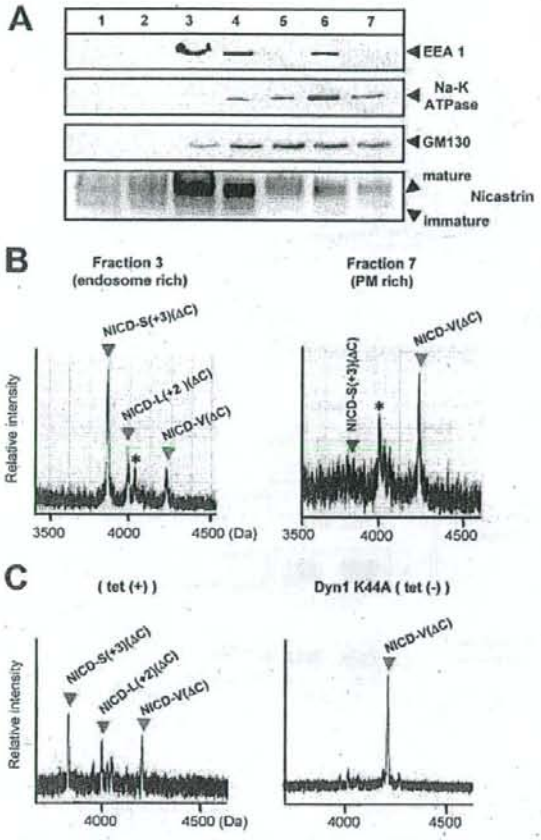

FIG. 6. Subcellular locations where S3-V and S3-S(+3) cleavages occur. (A) Fractions from a 2.5% to 25% linear iodixanol gradient examined by immunoblotting with the indicated antibodies. (B) MS spectra of NICD(ΔC) generated in the cell-free assay using membranes collected by centrifugation from the endosome-rich (fraction 3) and the PM-rich (fraction 7) fractions. Asterisks indicate nonspecific peaks. (C) MS spectra of NICD(ΔC) generated in the cell-free assay. CMFs from HeLa cells stably expressing NEXT(ΔC) and conditionally expressing Dyn-1 K44A were used. The precision of PS-dependent cleavage at the TM-cytoplasmic border in HeLa (left panel) and K293 (Fig. 1C) cells was different, in agreement with a previous report (11).

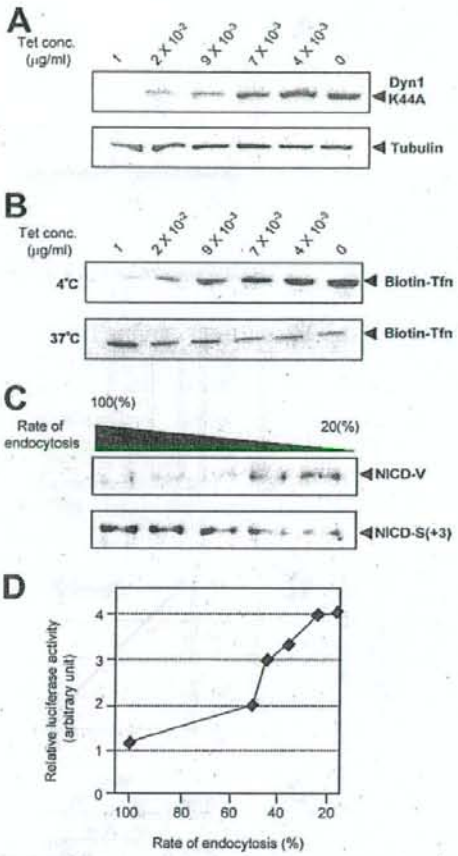

FIG. 7. Parallel change in the rate of endocytosis and the precision of S3 cleavage. (A) Expression of Dyn-1 K44A at various concentrations of tetracycline. Dyn-1 K44A/NEXT-coexpressing HeLa cells were cultured in medium with the indicated concentrations of tetracycline, and cell lysates were examined by immunoblotting with antibody 12CA5 (upper panel) or antitubulin (lower panel). The levels of Dyn-1 K44A increase as the concentration of tetracycline is decreased. (B) Various rates of endocytosis in Dyn-1 K44A expressing cells. Transferrin (Tfn) uptake assays were performed to measure the rate of endocytosis. The ratio of internalized Tfn (37°C; lower panel) to surface-bound Tfn (4°C; upper panel) in cells cultured in medium containing 1 μg/ml of tetracycline was defined as 100%. The rate of endocytosis decreased to ~15% when tetracycline was completely withdrawn. (C) Effect of the rate of endocytosis on the NICD species. The calculated rates of endocytosis were 100%, 41%, 37%, 21%, and 15% in lanes 1 to 5, respectively. (D) A plot of the relative Notch downstream luciferase activity versus the rate of endocytosis at various tetracycline concentrations.

mutant was found to be degraded mainly into NICD-L(+2)(ΔC), NICD-S(+3)(ΔC), and NICD-R(+5)(ΔC) species, which have unstable Leu1746, Ser1747, and the mutated Arg1749 at the N terminus, respectively (Fig. 8E). These results suggest that due to a dramatic change in the S3 cleavage precision, the Lys→Arg mutation causes not only a decrease of NICD-V but also an increase of extra unstable NICD species besides NICD-S(+3). This finding is reminiscent of the S3 cleavage for the Val→Gly mutant NEXT. Moreover, we studied whether NICDs in living cells expressing the Lys→Arg mutant are composed mainly of unstable NICD species. Strikingly, in the cells stably expressing the mutant NEXT, the stable NICD-V was barely detectable (13), while substantial amounts of NICDs were generated in the presence of the proteasome inhibitor mixture (Fig. 8F, top and middle panels). Since almost no NICD is observed in the mutant cells without the inhibitor mixture, it is indicated that NICDs in the Lys→Arg mutant-expressing cells are composed of unstable species (Fig. 8F, bottom panel). Therefore, the changes in the S3 cleavage precision induced by these S3 mutations are at

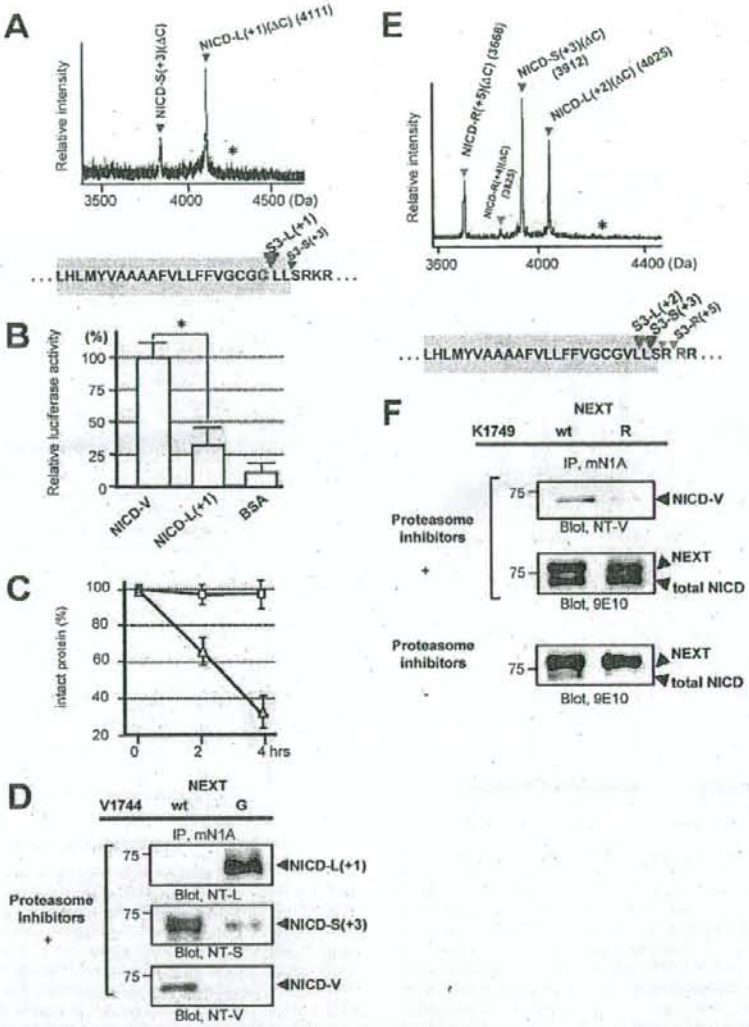

FIG. 8. Characteristics of the NICD species generated from the Val→Gly and the Lys→Arg mutants in cultured cells. (A) MS spectrum of de novo NICD(ΔC) generated from the Val→Gly mutant of NEXTΔC in K293 cells. The asterisk indicates the position of molecular mass corresponding to NICD-G(ΔC) species. Colored letters and inverted triangles show the mutation and proteolytic sites, respectively. (B) Assay of Notch downstream signaling induced by NICD-L(+1). Experiments were performed as described for Fig. 5B. The luciferase activity in the NICD-V-loaded cells was defined as 100%. Values represent means ± standard deviations. ($n = 3$). The asterisk indicates that the relative luciferase activity in NICD-V-loaded cells is statistically different than that in NICD-L(+1)-loaded cells ($P < 0.001$). (C) Degradation of NICD-L(+1) species in vitro. Experiments were performed as described for Fig. 5C but using NICD-L(+1) (triangles) and NICD-V (squares). Values represent means ± standard deviations ($n = 3$). (D) Generation of NICD-L(+1) and NICD-S(+3) in the Val→Gly mutant NEXT cells. K293 cells expressing either wt or the Val→Gly mutant NEXT were analyzed as described for Fig. 2D. (E) MS spectrum of de novo NICD(ΔC) generated from the Lys→Arg mutant of NEXTΔC in K293 cells. The asterisk indicates the position of molecular mass corresponding to NICD-V(ΔC) species. Colored letters and inverted triangles show the mutation and proteolytic sites, respectively. (F) Generation of unstable NICD species in the Lys→Arg mutant NEXT cells. K293 cells expressing either wt or the Lys→Arg mutant NEXT were analyzed as described for Fig. 2D (top and middle panels).

least partially responsible for the observed decrease in NICD level/Notch signaling in cultured cells.

Unlike several FAD-associated PS1 mutations, modifiers of PS/γ-secretase do not induce changes in the precision of S3 cleavage. Many FAD PS mutations affect the precision of not only γ but also ε cleavages of βAPP and, therefore, generally increase the relative AICDε48/AICDε49 ratio as well as the Aβ42/Aβ40 ratio (38, 42). In addition, compounds that modify the activity of PS/γ-secretase, including a subset of nonsteroidal anti-inflammatory drugs, cause reciprocal changes in rela-

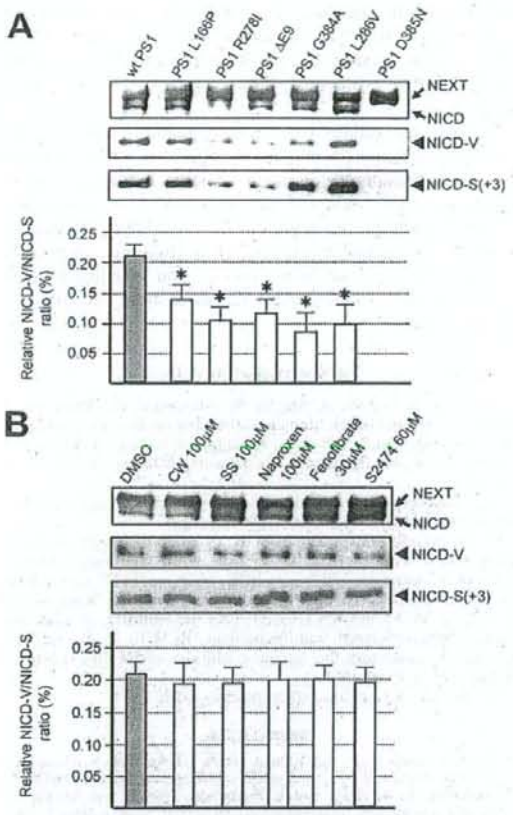

FIG. 9. Changes in the precision of S3 cleavage induced by FAD mutations in PS1. (A) Effect of several FAD PS1 mutations on the precision of S3 cleavage. K293 cells expressing the indicated PS mutant were transiently transfected with NEXT and analyzed as for Fig. 2D. The production of total NICD (first panel), NICD-V (second panel), and NICD-S(+3) (third panel) was assessed. Note that amount of total NICD was greatly reduced in PS1 R278I- and Δexon 9-expressing cells. The ratio of NICD-V to NICD-S(+3) in cells expressing wt PS1 or FAD mutants is shown in the bottom panel. Values represent means ± standard deviations ($n = 3$). The asterisk indicates that the ratio of NICD-V to NICD-S(+3) in cells expressing PS1 FAD mutants is significantly different from that in wt PS1-expressing cells ($P < 0.002$). (B) Effect of PS/γ-secretase modifiers on the precision of S3 cleavage. K293 cells stably expressing NEXT were treated with several PS/γ-secretase modifiers at the indicated concentration for 24 h and analyzed as described for the first three panels in panel A. DMSO, dimethyl sulfoxide; CW, compound W (31); SS, sulindac sulfide (49). The ratio of NICD-V to NICD-S(+3) in the control and treated cells is shown in the bottom panel. Values represent means ± standard deviations ($n = 3$).

tive production of Aβ42 and Aβ38 (19, 31, 49). Therefore, we investigated whether FAD PS mutations or PS/γ-secretase modifiers affect the precision of S3 cleavage. To evaluate the precision change, we used the relative NICD-V/NICD-S ratio, mimicking the relative Aβ42/Aβ40 ratio in the case of γ cleavage. Immunoblotting using anti-NT-V or anti-NT-S revealed that cells coexpressing PS1 mutants and NEXT produce both of the NICD species (Fig. 9A, top three panels). We found that the relative ratio of S3-V to S3-S(+3) cleavage was significantly reduced in some mutants (Fig. 9A, bottom panel). Subsequently, we examined the effects of PS/γ-secretase modifiers and naproxen (Fig. 9B). Because the effective doses of the compounds for γ and S3 cleavage may differ, we performed dose-response experiments to select the highest working concentrations (data not shown). After confirming that the level of Aβ42 in the medium was altered following a 24-h incubation with each compound (data not shown), we analyzed the cell lysates for the presence of NICD-V and NICD-S(+3) (Fig. 9B). In contrast to the case for the FAD mutants, the relative ratio of S3-V to S3-S(+3) cleavage was unchanged by the modifiers. These results suggest that γ-secretase modifiers do not affect the precision of intramembrane proteolysis by PS/γ-secretase.

DISCUSSION

The current studies suggest a novel mode by which the intensity of Notch signaling is regulated. We found that intracellular Notch signaling molecules (NICDs) in target cells can be divided into a stable one that transmits a substantial signal and unstable ones that transmit a much weaker signal, depending on the specific site of S3 cleavage. Therefore, Notch signaling intensity transmitted by conversion of extracellular signaling into intracellular signaling could depend on the characteristics of the target cell. For example, although S3 cleavage occurs, cells might not receive a substantial Notch signal when predominantly unstable NICDs are generated. On the basis of our results, we propose that the precision of S3 cleavage by PS/γ-secretase in the target cell is an important factor in determining the signaling intensity.

PS-dependent proteolysis on the TM of Notch-1 and βAPP consists of dual cleavage at the S4/S3 and γ/ε sites, respectively (14, 31, 33). The finding of diversity in the site of S3 cleavage means that cleavage at all four sites in the TM of Notch-1 and βAPP can vary. Thus, we suggest that the existence of variability in both the site and precision of cleavage may be a common feature of PS-dependent intramembrane proteolysis. Furthermore, we found that the precision of cleavage at S3 changes according to the subcellular location. On the PM, cleavage is more likely at S3-V, whereas on endosomes, cleavage is more likely at S3-S(+3), which is more C terminal. Interestingly, we have obtained very similar results regarding the cleavage of βAPP at the ε site (11). The precision of cleavage at the ε site changes depending on the subcellular location (11). The ε49 cleavage, which topologically corresponds to S3-V, occurs mainly on the PM, whereas the more C-terminal ε51 cleavage, which topologically corresponds to S3-S, occurs mainly on endosomes. Therefore, we have demonstrated that such subcellular location-dependent changes in the precision of the cleavage by PS/γ-secretase are common to the substrates. These findings suggest that such changes reflect a functional alteration of PS/γ-secretase in each subcellular location.

S2 cleavage upon ligand binding should occur on the PM of the target cells, but whether the subsequent S3 cleavage occurs on the PM or after endocytosis remains controversial (13, 17, 20, 46). The results of the current study suggest that (i) S3 cleavage occurs in both subcellular fractions in cell culture and

(ii) S3-V cleavage, which generates stable NICD-V, occurs predominantly on the PM, whereas S3-S(+3) cleavage, which generates unstable NICD-S(+3), occurs predominantly on endosomes. We also found that the intensity of Notch signaling changes along with the extent of endocytosis, perhaps due to a change in the precision of S3 cleavage. Therefore, our results suggest that NICD generation on the PM and endosomes increases and decreases the intensity of Notch signaling, respectively. Reports that Sanpodo positively regulates Notch signaling on the PM and that Numb, a negative regulator, promotes endocytosis of Notch receptors and/or Sanpodo are consistent with our findings (3, 28). A previous study showed that *Drosophila* with a mutation in *shibire*, which encodes a homolog of dynamin, has a phenotype indicating a loss of Notch function (43). Further study to solve the contradiction is necessary.

Elimination of either Notch or PS function causes a strong Notch loss-of-function phenotype in vivo (23, 41). Knock-in mice with the S3 (Val→Gly) mutant of Notch-1 display a hypomorphic Notch phenotype, possibly due to reduced Notch signaling caused by a decrease in the intracellular NICD level (6, 15, 39). This reduction in the level of NICD polypeptides could be due to decreased generation and/or increased degradation (4, 6). Previously, NICD was considered to be a single polypeptide mediating a single type of signaling, implying that the lower level of NICD is due to a decrease in its generation; however, we found that the N termini of NICDs may play critical roles in their stabilities and thus signaling intensities.

Among S3 mutants of Notch-1, the Lys→Arg mutant NEXT is neither monoubiquitinated at Arg1749 nor endocytosed (13). Concurrently, the NICD-V level in the cells expressing this mutant is low (13). In this paper, we demonstrated that the Lys→Arg mutation also causes a drastic change in the precision of the S3 cleavage, which results in a drastic decrease of NICD-V generation on the PM. This explanation, if valid, resolves the discrepancy between the two studies.

Both stabilizing (Val, Met, or Gly) and destabilizing amino acid residues seem to be conserved in Notch orthologs of various organisms (see Table S2 in the supplemental material). This suggests that both stable and unstable intracellular Notch signaling exists in many species. Previous studies have indicated that differences in the intensity, duration, and timing of Notch signaling in target cells affect cell fate decisions (7, 26). Furthermore, the signaling by a molecule is dependent on its lifetime in the cell, and the lifetime should be short enough for the target cell to be able to rapidly change the extent of signaling (22). Therefore, target cells in different contexts may convert extracellular signals to various relative amounts of short- and long-term Notch signals.

FAD PS mutations generally increase the generation of Aβ42 (42). This pathological gain of function of PS is due to a change in the precision of γ cleavage, resulting in an increase in cleavage at γ42 (42). PS/γ-secretase modifiers can up- or down-regulate the cleavage at γ42 (19, 31, 49). In both cases, the modifiers have reciprocal effects on the production of Aβ42 and Aβ38 (31, 49). In this study, we found that several FAD PS1 mutants change the precision of S3 cleavage but that the PS/γ-secretase modifiers do not. These findings are consistent with previous studies showing that the precision of ε cleavage in βAPP is altered by certain FAD PS mutations (38) and that Notch processing is unaffected by nonsteroidal anti-inflammatory drugs that can reduce Aβ42 generation (45, 49). PS/γ-secretase modifiers could thus affect the precision of the intramembrane proteolysis differently from PS FAD mutations.

Because up-regulation in Notch signaling is involved in a subset of malignancies (10, 37, 47, 50), γ-secretase inhibitors have been considered for the treatment of cancer; however, inhibitors would cause the accumulation of substrates (i.e., NEXT), inevitably producing a "rebound effect," where the concentration of NICD would increase. Therefore, compounds that alter the precision of S3 cleavage and specifically inhibit the generation of stable NICD-V may be more effective therapeutic agents.

ACKNOWLEDGMENTS

We thank J. Takeda, R. Kopan, M. Nishimura, H. Hasegawa, Y. Eguchi, Y. Tsujimoto, H. Steiner, and C. Haass for critically reading the manuscript and S. Shirahata, R. Kopan, J. S. Nye, A. Israel, S. L. Schmid, and G. W. Bornkamm for providing cDNAs, constructs, and cell lines.

M.O. conceived and designed the experiments. S.T. and others performed the experiments. M.O. wrote the paper.

We are grateful for funding from the Program for the Promotion of Fundamental Studies in Health Sciences of the National Institute of Biomedical Innovation (05-26) (to M.T., M.O., and S.T.), grants-in-aid for Scientific Research on Priority Areas-Advanced Brain Science Project (to M.O.) and KAKEN-HI from the Ministry of Education, Culture, Sports, Science, and Technology (to M.T., M.O., and S.T.), and grants-in-aid from the Japanese Ministry of Health, Labor and Welfare (to M.T. and M.O.).

We declare that no competing interests exist.

REFERENCES

1. **Artavanis-Tsakonas, S., M. D. Rand, and R. J. Lake.** 1999. Notch signaling: cell fate control and signal integration in development. Science **284:**770–776.
2. **Bachmair, A., D. Finley, and A. Varshavsky.** 1986. In vivo half-life of a protein is a function of its amino-terminal residue. Science **234:**179–186.
3. **Berdnik, D., T. Torok, M. Gonzalez-Gaitan, and J. A. Knoblich.** 2002. The endocytic protein alpha-adaptin is required for numb-mediated asymmetric cell division in Drosophila. Dev. Cell **3:**221–231.
4. **Blat, Y., J. E. Meredith, Q. Wang, J. D. Bradley, L. A. Thompson, R. E. Olson, A. M. Stern, and D. Seiffert.** 2002. Mutations at the P1′ position of Notch1 decrease intracellular domain stability rather than cleavage by gamma-secretase. Biochem. Biophys. Res. Commun. **299:**569–573.
5. **Cao, X., and T. C. Sudhof.** 2001. A transcriptionally active complex of APP with Fe65 and histone acetyltransferase Tip60. Science **293:**115–120.
6. **Chandu, D., S. S. Huppert, and R. Kopan.** 2006. Analysis of transmembrane domain mutants is consistent with sequential cleavage of Notch by gamma-secretase. J. Neurochem. **96:**228–235.
7. Reference deleted.
8. **De Strooper, B., W. Annaert, P. Cupers, P. Saftig, K. Craessaerts, J. S. Mumm, E. H. Schroeter, V. Schrijvers, M. S. Wolfe, W. J. Ray, A. Goate, and R. Kopan.** 1999. A presenilin-1-dependent gamma-secretase-like protease mediates release of Notch intracellular domain. Nature **398:**518–522.
9. **Fehon, R. G., K. Johansen, I. Rebay, and S. Artavanis-Tsakonas.** 1991. Complex cellular and subcellular regulation of notch expression during embryonic and imaginal development of Drosophila: implications for notch function. J. Cell Biol. **113:**657–669.
10. **Fre, S., M. Huyghe, P. Mourikis, S. Robine, D. Louvard, and S. Artavanis-Tsakonas.** 2005. Notch signals control the fate of immature progenitor cells in the intestine. Nature **435:**964–968.
11. **Fukumori, A., M. Okochi, S. Tagami, J. Jiang, N. Itoh, T. Nakayama, K. Yanagida, Y. Ishizuka-Katsura, T. Morihara, K. Kamino, T. Tanaka, T. Kudo, H. Tanii, A. Ikuta, C. Haass, and M. Takeda.** 2006. Presenilin-dependent gamma-secretase on plasma membrane and endosomes is functionally distinct. Biochemistry **45:**4907–4914.
12. **Gonda, D. K., A. Bachmair, I. Wunning, J. W. Tobias, W. S. Lane, and A. Varshavsky.** 1989. Universality and structure of the N-end rule. J. Biol. Chem. **264:**16700–16712.
13. **Gupta-Rossi, N., E. Six, O. LeBail, F. Logeat, P. Chastagner, A. Olry, A. Israel, and C. Brou.** 2004. Monoubiquitination and endocytosis direct gamma-secretase cleavage of activated Notch receptor. J. Cell Biol. **166:**73–83.

14. **Haass, C., and H. Steiner.** 2002. Alzheimer disease gamma-secretase: a complex story of GxGD-type presenilin proteases. Trends Cell Biol. **12**:556–562.
15. **Huppert, S. S., A. Le, E. H. Schroeter, J. S. Mumm, M. T. Saxena, L. A. Milner, and R. Kopan.** 2000. Embryonic lethality in mice homozygous for a processing-deficient allele of Notch1. Nature **405**:966–970.
16. **Jarriault, S., C. Brou, F. Logeat, E. H. Schroeter, R. Kopan, and A. Israel.** 1995. Signalling downstream of activated mammalian Notch. Nature **377**:355–358.
17. **Kaether, C., S. Schmitt, M. Willem, and C. Haass.** 2006. Amyloid precursor protein and Notch intracellular domains are generated after transport of their precursors to the cell surface. Traffic **7**:408–415.
18. **Koo, E. H., and R. Kopan.** 2004. Potential role of presenilin-regulated signaling pathways in sporadic neurodegeneration. Nat. Med. **10**(Suppl.):S26–S33.
19. **Kukar, T., M. P. Murphy, J. L. Eriksen, S. A. Sagi, S. Weggen, T. E. Smith, T. Ladd, M. A. Khan, R. Kache, J. Beard, M. Dodson, S. Merit, V. V. Ozols, P. Z. Anastasiadis, P. Das, A. Fauq, E. H. Koo, and T. E. Golde.** 2005. Diverse compounds mimic Alzheimer disease-causing mutations by augmenting Abeta42 production. Nat. Med. **11**:545–550.
20. **Lopez-Schier, H., and D. St. Johnston.** 2002. Drosophila nicastrin is essential for the intramembranous cleavage of notch. Dev. Cell **2**:79–89.
21. **Minoguchi, S., Y. Taniguchi, H. Kato, T. Okazaki, L. J. Strobl, U. Zimber-Strobl, G. W. Bornkamm, and T. Honjo.** 1997. RBP-L, a transcription factor related to RBP-Jκ. Mol. Cell. Biol. **17**:2679–2687.
22. **Morimoto, M., Y. Takahashi, M. Endo, and Y. Saga.** 2005. The Mesp2 transcription factor establishes segmental borders by suppressing Notch activity. Nature **435**:354–359.
23. **Mumm, J. S., and R. Kopan.** 2000. Notch signaling: from the outside in. Dev. Biol. **228**:151–165.
24. **Mumm, J. S., E. H. Schroeter, M. T. Saxena, A. Griesemer, X. Tian, D. J. Pan, W. J. Ray, and R. Kopan.** 2000. A ligand-induced extracellular cleavage regulates gamma-secretase-like proteolytic activation of Notch1. Mol. Cell **5**:197–206.
25. **Munter, L. M., P. Voigt, A. Harmeier, D. Kaden, K. E. Gottschalk, C. Weise, R. Pipkorn, M. Schaefer, D. Langosch, and G. Multhaup.** 2007. GxxxG motifs within the amyloid precursor protein transmembrane sequence are critical for the etiology of Abeta42. EMBO J. **26**:1702–1712.
26. **Nakagawa, M., M. Ichikawa, K. Kumano, S. Goyama, M. Kawazu, T. Asai, S. Ogawa, M. Kurokawa, and S. Chiba.** 2006. AML1/Runx1 rescues Notch1-Null mutation-induced deficiency of para-aortic splanchnopleural hematopoiesis. Blood **108**:3329–3334.
27. **Nakaya, Y., T. Yamane, H. Shiraishi, H. Q. Wang, E. Matsubara, T. Sato, G. Dolios, R. Wang, B. De Strooper, M. Shoji, H. Komano, K. Yanagisawa, Y. Ihara, P. Fraser, P. St George-Hyslop, and M. Nishimura.** 2005. Random mutagenesis of presenilin-1 identifies novel mutants exclusively generating long amyloid beta-peptides. J. Biol. Chem. **280**:19070–19077.
28. **O'Connor-Giles, K. M., and J. B. Skeath.** 2003. Numb inhibits membrane localization of Sanpodo, a four-pass transmembrane protein, to promote asymmetric divisions in Drosophila. Dev. Cell **5**:231–243.
29. **Ohashi, H., and T. Sudo.** 1994. Efficient expression of a transfected foreign gene by Cos1 cells in serum-free medium. Biosci. Biotechnol. Biochem. **58**:758–759.
30. **Okochi, M., S. Eimer, A. Bottcher, R. Baumeister, H. Romig, J. Walter, A. Capell, H. Steiner, and C. Haass.** 2000. A loss of function mutant of the presenilin homologue SEL-12 undergoes aberrant endoproteolysis in Caenorhabditis elegans and increases abeta 42 generation in human cells. J. Biol. Chem. **275**:40925–40932.
31. **Okochi, M., A. Fukumori, J. Jiang, N. Itoh, R. Kimura, H. Steiner, C. Haass, S. Tagami, and M. Takeda.** 2006. Secretion of the Notch-1 Abeta-like peptide during Notch signaling. J. Biol. Chem. **281**:7890–7898.
32. **Okochi, M., K. Ishii, M. Usami, N. Sahara, F. Kametani, K. Tanaka, P. E. Fraser, M. Ikeda, A. M. Saunders, L. Hendriks, S. I. Shoji, L. E. Nee, J. J. Martin, C. Van Broeckhoven, P. H. St George-Hyslop, A. D. Roses, and H. Mori.** 1997. Proteolytic processing of presenilin-1 (PS-1) is not associated with Alzheimer's disease with or without PS-1 mutations. FEBS Lett. **418**:162–166.
33. **Okochi, M., H. Steiner, A. Fukumori, H. Tanii, T. Tomita, T. Tanaka, T. Iwatsubo, T. Kudo, M. Takeda, and C. Haass.** 2002. Presenilins mediate a dual intramembranous gamma-secretase cleavage of Notch-1. EMBO J. **21**:5408–5416.
34. **Okochi, M., J. Walter, A. Koyama, S. Nakajo, M. Baba, T. Iwatsubo, L. Meijer, P. J. Kahle, and C. Haass.** 2000. Constitutive phosphorylation of the Parkinson's disease associated alpha-synuclein. J. Biol. Chem. **275**:390–397.
35. **Parks, A. L., K. M. Klueg, J. R. Stout, and M. A. Muskavitch.** 2000. Ligand endocytosis drives receptor dissociation and activation in the Notch pathway. Development **127**:1373–1385.
36. **Qi-Takahara, Y., M. Morishima-Kawashima, Y. Tanimura, G. Dolios, N. Hirotani, Y. Horikoshi, F. Kametani, M. Maeda, T. C. Saido, R. Wang, and Y. Ihara.** 2005. Longer forms of amyloid beta protein: implications for the mechanism of intramembrane cleavage by gamma-secretase. J. Neurosci. **25**:436–445.
37. **Radtke, F., and K. Raj.** 2003. The role of Notch in tumorigenesis: oncogene or tumour suppressor? Nat. Rev. Cancer **3**:756–767.
38. **Sato, T., N. Dohmae, Y. Qi, N. Kakuda, H. Misonou, R. Mitsumori, H. Maruyama, E. H. Koo, C. Haass, K. Takio, M. Morishima-Kawashima, S. Ishiura, and Y. Ihara.** 2003. Potential link between amyloid beta-protein 42 and C-terminal fragment gamma 49–99 of beta-amyloid precursor protein. J. Biol. Chem. **278**:24294–24301.
39. **Schroeter, E. H., J. A. Kisslinger, and R. Kopan.** 1998. Notch-1 signalling requires ligand-induced proteolytic release of intracellular domain. Nature **393**:382–386.
40. **Schweisguth, F.** 2004. Notch signaling activity. Curr. Biol. **14**:R129–R138.
41. **Selkoe, D., and R. Kopan.** 2003. Notch and Presenilin: regulated intramembrane proteolysis links development and degeneration. Annu. Rev. Neurosci. **26**:565–597.
42. **Selkoe, D. J.** 2001. Alzheimer's disease: genes, proteins, and therapy. Physiol. Rev. **81**:741–766.
43. **Seugnet, L., P. Simpson, and M. Haenlin.** 1997. Requirement for dynamin during Notch signaling in Drosophila neurogenesis. Dev. Biol. **192**:585–598.
44. **Steiner, H., M. Kostka, H. Romig, G. Basset, B. Pesold, J. Hardy, A. Capell, L. Meyn, M. L. Grim, R. Baumeister, K. Fechteler, and C. Haass.** 2000. Glycine 384 is required for presenilin-1 function and is conserved in bacterial polytopic aspartyl proteases. Nat. Cell Biol. **2**:848–851.
45. **Takahashi, Y., I. Hayashi, Y. Tominari, K. Rikimaru, Y. Morohashi, T. Kan, H. Natsugari, T. Fukuyama, T. Tomita, and T. Iwatsubo.** 2003. Sulindac sulfide is a noncompetitive gamma-secretase inhibitor that preferentially reduces Abeta 42 generation. J. Biol. Chem. **278**:18664–18670.
46. **Tarassishin, L., Y. I. Yin, B. Bassit, and Y. M. Li.** 2004. Processing of Notch and amyloid precursor protein by gamma-secretase is spatially distinct. Proc. Natl. Acad. Sci. USA **101**:17050–17055.
47. **van Es, J. H., M. E. van Gijn, O. Riccio, M. van den Born, M. Vooijs, H. Begthel, M. Cozijnsen, S. Robine, D. J. Winton, F. Radtke, and H. Clevers.** 2005. Notch/gamma-secretase inhibition turns proliferative cells in intestinal crypts and adenomas into goblet cells. Nature **435**:959–963.
48. **Washburn, T., E. Schweighoffer, T. Gridley, D. Chang, B. J. Fowlkes, D. Cado, and E. Robey.** 1997. Notch activity influences the alphabeta versus gammadelta T cell lineage decision. Cell **88**:833–843.
49. **Weggen, S., J. L. Eriksen, P. Das, S. A. Sagi, R. Wang, C. U. Pietrzik, K. A. Findlay, T. E. Smith, M. P. Murphy, T. Bulter, D. E. Kang, N. Marquez-Sterling, T. E. Golde, and E. H. Koo.** 2001. A subset of NSAIDs lower amyloidogenic Abeta42 independently of cyclooxygenase activity. Nature **414**:212–216.
50. **Weng, A. P., A. A. Ferrando, W. Lee, J. P. t. Morris, L. B. Silverman, C. Sanchez-Irizarry, S. C. Blacklow, A. T. Look, and J. C. Aster.** 2004. Activating mutations of NOTCH1 in human T cell acute lymphoblastic leukemia. Science **306**:269–271.
51. **Wolfe, M. S., W. Xia, B. L. Ostaszewski, T. S. Diehl, W. T. Kimberly, and D. J. Selkoe.** 1999. Two transmembrane aspartates in presenilin-1 required for presenilin endoproteolysis and gamma-secretase activity. Nature **398**:513–517.
52. **Xia, W., and M. S. Wolfe.** 2003. Intramembrane proteolysis by presenilin and presenilin-like proteases. J. Cell Sci. **116**:2839–2844.
53. **Zhao, G., M. Z. Cui, G. Mao, Y. Dong, J. Tan, L. Sun, and X. Xu.** 2005. Gamma-cleavage is dependent on zeta-cleavage during the proteolytic processing of amyloid precursor protein within its transmembrane domain. J. Biol. Chem. **280**:37689–37697.

J Hum Genet (2008) 53:296–302
DOI 10.1007/s10038-008-0251-9

ORIGINAL ARTICLE

Dynamin 2 gene is a novel susceptibility gene for late-onset Alzheimer disease in non-*APOE*-ε4 carriers

Nuripa Jenishbekovna Aidaralieva · Kouzin Kamino · Ryo Kimura · Mitsuko Yamamoto · Takeshi Morihara · Hiroaki Kazui · Ryota Hashimoto · Toshihisa Tanaka · Takashi Kudo · Tomoyuki Kida · Jun-Ichiro Okuda · Takeshi Uema · Hidehisa Yamagata · Tetsuro Miki · Hiroyasu Akatsu · Kenji Kosaka · Masatoshi Takeda

Received: 6 November 2007 / Accepted: 30 December 2007 / Published online: 31 January 2008

Abstract Alzheimer disease (AD) is characterized by progressive cognitive decline caused by synaptic dysfunction and neurodegeneration in the brain, and late-onset AD (LOAD), genetically classified as a polygenetic disease, is the major form of dementia in the elderly. It has been shown that β amyloid, deposited in the AD brain, interacts with dynamin 1 and that the dynamin 2 (*DNM2*) gene homologous to the dynamin 1 gene is encoded at chromosome 19p13.2 where a susceptibility locus has been detected by linkage analysis. To test the genetic association of LOAD with the *DNM2* gene, we performed a case–control study of 429 patients with LOAD and 438 sex- and age-matched control subjects in a Japanese population. We found a significant association of LOAD with single nucleotide polymorphism markers of the *DNM2* gene, especially in non-carriers of the apolipoprotein E-ε4 allele. Even though subjects with the genotype homozygous for the risk allele at rs892086 showed no mutation in exons of the *DNM2* gene, expression of *DNM2* mRNA in the hippocampus was decreased in the patients compared to non-demented controls. We propose that the *DNM2* gene is a novel susceptibility gene for LOAD.

Keywords Alzheimer · Apolipoprotein E · Association · Chromosome 19p · Dynamin 2 · Genetic risk

Electronic supplementary material The online version of this article (doi:10.1007/s10038-008-0251-9) contains supplementary material, which is available to authorized users.

N. J. Aidaralieva · K. Kamino (✉) · R. Kimura · M. Yamamoto · T. Morihara · H. Kazui · R. Hashimoto · T. Tanaka · T. Kudo · M. Takeda
Department of Psychiatry,
Osaka University Graduate School of Medicine,
Suita, Osaka 565-0871, Japan
e-mail: kkamino@psy.med.osaka-u.ac.jp

K. Kamino · T. Kida · J.-I. Okuda
Shoraiso National Hospital, Yamatokoriyama, Nara, Japan

T. Uema
Department of Psychiatry, Osaka General Medical Center,
Osaka, Japan

H. Yamagata
Department of Preventive Medicine,
Ehime University Graduate School of Medicine,
Toon, Ehime, Japan

T. Miki
Department of Geriatric Medicine,
Ehime University Graduate School of Medicine,
Toon, Ehime, Japan

H. Akatsu · K. Kosaka
Choju Medical Institute, Fukushimura Hospital,
Toyohashi, Aichi, Japan

Introduction

Alzheimer disease (AD) is the most common form of dementia in the elderly and is characterized by progressive cognitive decline with brain atrophy that is most marked in the temporal lobes. It is thought that β amyloid is a causative molecule in AD by disturbing synaptic function, leading to neuronal death (for review, see Selkoe 2002; Yao 2004). Although both early- and late-onset AD (LOAD) exhibit the same neuropathology in the brain, LOAD is genetically classified as a polygenetic disease and is characterized by more heterogeneous conditions than autosomal dominant early-onset AD. Apolipoprotein E (*APOE*) has been shown to be a major risk factor for LOAD (Corder et al. 1993; Farrer et al. 1997). Genome scans of LOAD detected several susceptibility loci, among

which chromosomes 12, 10 and 9 have been the targets of searches for risk genes (Pericak-Vance et al. 1997; Blacker et al. 2003). Multipoint linkage analysis of LOAD families have also demonstrated a susceptibility locus at 19p13.2 between D19S391and D19S914 (Wijsman et al. 2004).

The major role of the dynamin proteins is in the endocytosis of vesicles, and its functions in vesicle budding have been described as being responsible for the constriction of the lipid neck, fission of lipids and regulation of the scission reaction (for review, see Praefcke and McMahon 2004). Expression of the dynamin 2 (*DNM2*) as well as dynamin 1 (*DNM1*) gene is downregulated by β amyloid in hippocampal neurons (Kelly et al. 2005), suggesting that the dynamin proteins are involved in the cascade of neurodegeneration caused by β amyloid. The dynamin-binding protein (*DNMBP*) gene on chromosome 10 has also been shown to be associated with LOAD (Kuwano et al. 2006). We observed that the *DNM2* gene is located at 19p13.2, within the region where a susceptibility locus was noted (Wijsman et al. 2004). Therefore, the *DNM2* gene could be a positional and functional candidate for a genetic risk for LOAD.

To examine whether the *DNM2* gene is genetically associated with LOAD, we performed an age- and sex-matched case–control study in a Japanese population. We propose herein that the *DNM2* gene is a novel genetic factor for LOAD in non-*APOE*-ε4 carriers.

Subjects and methods

Study subjects

Patients with LOAD were diagnosed as having definite or probable AD according to the criteria of the National Institute of Neurological and Communicative Disorders and Stroke–Alzheimer's Disease and Related Disorders Association (NINCDS–ADRDA) (McKhann et al. 1984). Controls consisted of non-demented elderly subjects obtained from the general population. Written informed consent to participate in this study was obtained, and then peripheral blood was drawn and subjected to DNA extraction. For a definite diagnosis of AD, dissections were carried out at the Choju Medical Institute after obtaining the agreement of the patients' guardians for diagnosis and genomic research. In total, 429 (69.9% female) patients participated in the study, of whom 66 had definite AD and 363 had probable AD. The mean age $\pm$ SD of the patient population at onset was 72.3 $\pm$ 8.1 years (range 60–94 years), and the mean age at blood drawing was 77.4 $\pm$ 8.7 years (range 60–98 years). The controls consisted of 438 individuals (63.7% female). The mean age of the controls at assessment was 74.5 $\pm$ 5.5 years (range 60–99 years). The age at onset of the patient was matched to the age of controls, and the sex composition was not different between the groups. Hippocampal tissue was also obtained from the postmortem brains of 22 patients with AD (age 82.8 $\pm$ 8.5 years, 63.6% female) and 12 controls (age 89.0 $\pm$ 7.0 years, age at onset 72.9 $\pm$ 7.2 years, 58.0% female). DNA was extracted from peripheral blood using a QIAamp DNA Blood Kit (Qiagen, Tokyo, Japan) and from brain tissue by the phenol–chloroform method (Sambrook et al. 1989). The procedure to obtain the specimens was approved by the Genome Ethical Committee of Osaka University Graduate School of Medicine, Ehime University, and the Choju Medical Institute of Fukushimura Hospital.

Genotyping and sequencing

Single nucleotide polymorphisms (SNPs) in the *DNM2* gene regions used in this study are listed in Table 1. Genotyping was performed by a quantitative genotyping method using the TaqMan SNP Genotyping System (Applied Biosystems, Foster City, CA). The genotype of the *APOE* gene was determined by a PCR-restriction fragment length polymorphism (RFLP) method (Wenham et al. 1991). DNA obtained from six patients and three controls homozygous for the risk allele at rs892086 of the *DNM2* gene was subjected to direct sequencing of its exons using the primers listed in Electronic Supplementary Material.

Quantitative real-time PCR

Total RNA was isolated from frozen hippocampal tissues using the acid guanidine–phenol–chloroform RNA extraction method provided as ISOGEN (Nippon Gene, Toyama, Japan) and purified using an RNeasy Mini kit (Qiagen, Valencia, CA). RNA samples with an A_{260}/A_{280} absorption ratio over 1.9 were subjected to cDNA synthesis using a High-Capacity cDNA Archive kit (Applied Biosystems). Primers and probe sets for the human *DNM2* and *β-actin* genes were purchased from TaqMan Gene Expression Assay products (Applied Biosystems), and quantitative real-time PCR was carried out in an ABI PRISM 7900HT (Applied Biosystems). All quantitative PCR reactions were duplicated, and the ratio of the amount of *DNM2* cDNA to that of the *β-actin* internal control cDNA was determined at the cycle threshold (CT).

Statistical analysis

Linkage disequilibrium (LD) between all pairs of biallelic loci was measured by Lewontin's D′ (|D′|) (Hedrick 1987)

Table 1 Single nucleotide polymorphism (SNP) markers in the *DNM2* gene

NCBI SNP reference ID	Location in NCBI (build 36.1)	Location	SNP sequence (allele ½)	Strand/ orientation	Minor allele
rs12974306	10691281	Intron 1	CTCTT[G/T]CCTTT	fwd/B	Allele 2
rs714307	10696405	Intron 1	CGCTA[C/T]TGCTG	fwd/B	Allele 1
rs892086	10698677	Intron 1	GTTAG[A/G]TACCA	rev/T	Allele 1
rs34626880	10701428	Intron 1	AGCTC[C/T]ACCTG	fwd/B	Allele 2
rs10775614	10728219	Intron 1	GGCAC[A/ G]TGGCG	fwd/T	Allele 2
rs7246673	10737841	Intron 2	AACCC[G/T]GCTGT	fwd/B	Allele 1
rs3826803	10744126	Intron 2	TTTCT[C/G]ATTTT	fwd/B	Allele 2
rs2043332	10752239	Intron 5	GTGAC[A/C]TCAGG	rev/T	Allele 1
rs873016	10755728	Intron 6	AAATG[A/G]TATTA	rev/T	Allele 1
rs1109376	10775829	Intron 12	AGGAT[A/G]CTTCT	fwd/T	Allele 1
rs3786719	10788100	intron 15	TGGAA[C/G]CTTCC	fwd/T	Allele 2
rs11085748	10788540	intron 15	GTTTT[C/T]CTCAT	fwd/B	Allele 2
rs3760781	10808522	3'UTR	TTGAG[C/T]GCTCA	fwd/B	Allele 2

UTR, Untranslated region; NCBI, National Center for Biotechnology Information

and r^2. Haplotype blocks, defined as segments with strong LD (Gabriel et al 2002), were calculated using HAPLOVIEW (Barrett et al. 2005). Allele and genotype frequencies were assessed for associations by one-sided chi-squared test for both allele and genotype frequencies in dominant and recessive models, where p values less than 0.05 were tentatively judged to be significant. The effective number of independent marker loci in the *DNM2* gene was calculated to correct for multiple testing, using the software SNPSPD (http://www.genepi.qimr.edu.au/general/daleN/SNPSpD/) based on the spectral decomposition of matrices of pair-wise LD between SNPs (Nyholt 2004). The experiment-wide significance threshold required to keep the type I error rate at 5% was used for judging significance to correct for multiple testing. The values obtained by quantitative PCR, having a normal distribution, were compared by Student's t test, and a p value less than 0.05 was considered to be significant.

Results

We genotyped 13 SNPs located from intron 1 to the 3′-untranslated region (UTR) of the *DNM2* gene (Table 1). In total, 429 cases and 438 sex- and age-matched controls were genotyped, and their genotype distributions of both the cases and controls were in Hardy–Weinberg equilibrium. In these datasets, the *APOE-ε4* allele was associated with LOAD ($p < 1 \times 10^{-10}$): compared to non-*APOE-ε4* carriers, the odds ratio for carrying one *APOE-ε4* allele was 4.3 [95% confidence interval (CI) 3.12–6.16] and that for carrying two *APOE-ε4* allele was 28.4 (95% CI 6.75–119). Linkage disequilibrium statistics indicated more than three haplotype blocks in the *DNM2* gene region (Fig. 1). No validated SNPs were available between rs873016 and rs1109376 at a distance of approximately 20 kb, and no strong evidence of LD was found between these two SNPs. The case–control study showed that p values of less than 0.05 were found in four SNPs located from intron 6 to the 3′UTR in terms of allele distribution, and in seven SNPs from intron 1 to the 3′UTR in terms of genotype frequencies; their odds ratios were between 1.53 and 1.75 (Table 2). Calculations with SNPSPD indicated that the effective number of independent marker loci was 8.3094 and that the experiment-wide significance threshold was 0.006. Therefore, rs3760781 remained significant after the correction for multiple testing ($p = 0.003$). To examine the interaction between the *DNM2* gene and the *APOE* gene, the cases and controls were divided into *APOE-ε4* carriers and non-*APOE-ε4* carriers. In non-*APOE-ε4* carriers, seven markers showed p values of less than 0.05, and the experiment-wide significance threshold (0.0059) supported a significant association at rs892086 ($p = 0.003$) as well as at rs3760781 ($p = 0.004$) (Table 3). However, no association was found in *APOE-ε4* carriers (data not shown), indicating that the association of the *DNM2* gene is specific for non-*APOE-ε4* carriers in our dataset.

To examine whether patients with the risk genotype could harbor any mutations in the *DNM2* gene, we sequenced all exons of the *DNM2* gene in patients and controls homozygous for the risk allele at rs892086, but we did not found any mutations, indicating that no particular mutation resulting in amino acid change is linked to the risk genotype of the *DNM2* gene. To examine the expression of the *DNM2* gene in the AD hippocampal tissue, we measured the amount of *DNM2* cDNA normalized to that of *β-actin* cDNA using quantitative PCR. Analysis of ten LOAD and eight control subjects revealed that there was significantly lower amounts of *DNM2* mRNA in the AD hippocampal tissue than in the controls ($p < 0.01$) (Fig. 2).

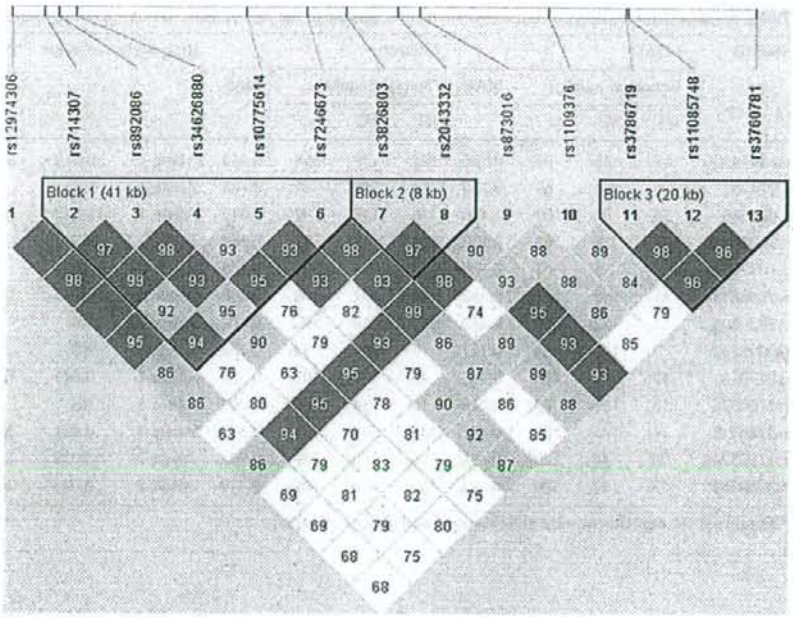

Fig. 1 Linkage disequilibrium coefficients and haplotype blocks in the *DNM2* gene region. Linkage disequilibrium coefficients (ID'I) among *DNM2* single nucleotide polymorphisms (SNPs) and haplotype blocks defined by strong LD are shown

Table 2 Association analysis of late-onset Alzheimer disease in the *DNM2* gene

SNP ID	LOAD				Control				Risk allele	*p* value	Risk genotype	*p* value	O.R (95% CI)
	Genotype number			MAF	Genotype number			MAF					
Genotype	1/1	2/2	½		1/1	2/2	½						
MArs12974306	174	57	196	0.363	204	46	188	0.320	Allele 2	NS	–	NS	
rs714307	16	285	127	0.186	16	304	117	0.170	Allele 1	NS	–	NS	
rs892086	93	134	202	0.452	67	145	226	0.411	Allele 1	NS	1/1	0.015	1.53 (1.08–2.17)
rs34626880	284	16	129	0.188	306	16	116	0.169	Allele 2	NS	–	NS	
rs10775614	306	11	111	0.155	326	14	95	0.141	Allele 2	NS	–	NS	
rs7246673	78	134	215	0.434	55	150	233	0.392	Allele 1	NS	1/1	0.020	1.56 (1.07–2.26)
rs3826803	132	86	209	0.446	145	58	234	0.400	Allele 2	NS	2/2	0.007	1.65 (1.15–2.37)
rs2043332	15	295	118	0.173	11	309	118	0.160	Allele 1	NS	–	NS	
rs873016	80	135	212	0.436	55	153	230	0.388	Allele 1	0.045	1/1	0.012	1.61 (1.11–2.33)
rs1109376	28	256	144	0.234	19	275	144	0.208	Allele 1	NS	–	NS	
rs3786719	145	85	198	0.430	166	57	215	0.376	Allele 2	0.021	2/2	0.007	1.66 (1.15–2.39)
rs11085748	138	81	209	0.433	160	56	222	0.381	Allele 2	0.027	2/2	0.013	1.59 (1.10–2.31)
rs3760781	141	87	199	0.437	157	56	225	0.385	Allele 2	0.028	2/2	0.003*	1.75 (2.21–2.52)

*Significant for experiment-wide significance threshold ($p < 0.006$)

LOAD, Late-onset Alzheimer disease; MAF, Minor Allele Frequency; O.R., odds ratio; 95% CI, 95% confidence interval

Discussion

We found that the *DNM2* gene is genetically associated with LOAD and that this association was specifically significant in non-*APOE*-ε4 carriers. In non-*APOE*-ε4 carriers, two SNPs, not in strong LD, were associated with LOAD. The *DNMBP* gene, which encodes a scaffold protein that binds to DNM1 protein, has been shown to be associated with LOAD in *APOE*-ε3*3 carriers or non-*APOE*-ε4 carriers, but not in *APOE*-ε4 carriers (Kuwano et al. 2006). Therefore, DNM2 protein could interact with proteins encoded in or linked to the *APOE*-ε3 genotype. It is

Table 3 Association analysis of late-onset Alzheimer disease in the *DNM2* gene in non-*APOE*-ε4 carriers

SNP ID	LOAD				Control				Risk allele	*p* value	Risk genotype	*p* value	O.R. (95% CI)
	Genotype number			MAF	Genotype number			MAF					
	1/1	2/2	½		1/1	2/2	½						
rs12974306	87	35	97	0.381	174	37	158	0.314	Allele 2	0.019	2/2	0.033	1.71 (1.04–2.80)
rs714307	6	152	63	0.170	12	259	97	0.164	Allele 1	NS		NS	
rs892086	55	64	102	0.480	56	121	192	0.412	Allele 1	0.023	1/1	0.003*	1.85 (1.22–2.81)
rs34626880	152	6	63	0.170	260	12	97	0.164	Allele 2	NS		NS	
rs10775614	164	5	51	0.139	278	11	77	0.135	Allele 2	NS		NS	
rs7246673	41	62	117	0.452	46	127	196	0.390	Allele 1	0.037	1/1	0.041	1.61 (1.02–2.54)
rs3826803	63	42	115	0.452	121	49	198	0.402	Allele 2	NS		NS	
rs2043332	7	149	64	0.177	7	264	98	0.152	Allele 1	NS		NS	
rs873016	42	63	116	0.452	46	130	193	0.386	Allele 1	0.025	1/1	0.031	1.65 (1.04–2.60)
rs1109376	13	138	69	0.216	15	234	120	0.203	Allele 1	NS		NS	
rs3786719	71	45	104	0.441	141	47	181	0.373	Allele 2	0.021	2/2	0.013	1.76 (1.13–2.76)
rs11085748	68	44	109	0.446	136	46	187	0.378	Allele 2	0.022	2/2	0.015	1.75 (1.11–2.74)
rs3760781	73	47	100	0.441	135	46	188	0.379	Allele 2	0.037	2/2	0.004*	1.91 (1.22–2.98)

*Significant for experiment-wide significance threshold ($p < 0.0059$)

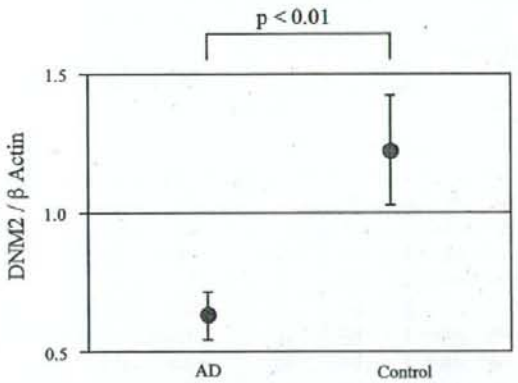

Fig. 2 Expression of *DNM2* mRNA in the hippocampus. The ratio of the amount of *DNM2* cDNA to that of *β-actin* cDNA is shown. *Dots* indicate mean value, *bars* indicate standard error

possible that the causative mechanism of DNM2 for the development of AD could be different from the lipid transfer proteins involved in lipid metabolism, such as the *APOE* (Strittmatter et al. 1993), *LRP* (Kang et al. 1997) and *CYP46* genes encoding cholesterol 24S-hydroxylase (Kolsch et al. 2002). However, the majority of cases genotyped in our study are still living, and the use of still living controls also warrants caution as the incidence of developing dementia increases with age. Therefore, our results could be misrepresented, as the controls may still develop AD, or we may have misdiagnosed AD patients who may actually have another form of dementia.

The *DNM* gene was first identified as the locus for a paralytic phenotype in *Drosophila melanogaster* (Suzuki et al. 1971) and encodes large GTPases that can associate with microtubules in vitro (Shpetner and Vallee 1989; Obar et al. 1990). The dynamin proteins are distinguished from other GTPases by their low GTP-binding affinities and the ability of many members of the dynamin family to interact with lipid membranes (for review, see Praefcke and McMahon 2004). Mutations of the pleckstrin homology domain of the *DNM2* gene, leading to diminished binding of the DNM2 protein to membranes, are responsible for Charcot–Marie-Tooth disease (Zuchner et al. 2005). While Charcot–Marie-Tooth disease is clinically characterized by peripheral neuropathy, the relation between aging and *DNM2* gene expression remains undetermined. Disuse muscle atrophy related to decreased daily activity is commonly found in the elderly, but it is unclear whether exercise is effective for the maintenance of cognitive function.

Kelly et al. (2005) showed that β amyloid induces depletion of the DNM1 as well as DNM2 protein in cultured hippocampal neurons and the hippocampus of a Tg2576 mouse model of AD. On the other hand, dominant-negative DNM1, which selectively inhibits receptor-mediated endocytosis, raises the levels of mature amyloid precursor protein (APP) at the cell-surface, which is consistent with retention of APP on the plasma membrane, and endogenous Aβ secretion was significantly increased (Chyung and Selkoe 2003). It has also been shown that the location of β amyloid can be changed by decreased activity

of the DNM1 protein and that endocytosis affects the precision of PS-dependent epsilon-cleavage in cell culture (Fukumori et al. 2006). Whereas the DNM1 protein is specific for presynaptic terminals in the central nervous system (CNS), the DNM2 protein is ubiquitously expressed and, to our knowledge, does not exist in presynaptic terminals in the CNS. However, DNM2 has a similar structure to DNM1 and might also affect the sequestration and scavenging of β amyloid in relation to its axonal transport in peripheral nervous system.

We found that the expression of hippocampal *DNM2* mRNA was lower in the patients than in the control subjects, but this result should be carefully interpreted. We examined a small number of hippocampal tissue samples and used *β-actin* cDNA as an internal control; however, quantitative PCR revealed that the *β-actin* transcript is differently expressed in brain specimens of AD and control subjects (Gutala and Reddy 2004). Therefore, this decrease should be examined in the other brain areas and also in a larger number of samples using another internal control cDNA, such as *GAPDH* (Gutala and Reddy 2004). Alternatively, *DNM2* gene expression could be depleted in AD due to the widespread devastation of neurons, particularly in the hippocampus, as well as by β amyloid. Therefore, it remains to be determined whether the decrease in *DNM2* expression is the cause or the outcome of AD.

Acknowledgments We thank Drs. Y. Ikejiri, T. Nishikawa, H. Yoneda, Y. Moto, A. Sawa, S. Fujinaga, T. Matsubayashi, K. Taniguchi, Y. Ikemura and T. Mori for clinical evaluations, and E. Miyamura for assistance. This work was funded by the Future Program and the Japan Society for the Promotion of Science (JSPS), and by a Grant-in-Aid for Scientific Research on Priority Areas "Applied Genomics" from the Ministry of Education, Culture, Sports, Science and Technology of Japan.

References

Barrett JC, Fry B, Maller J, Daly MJ (2005) Haploview: analysis and visualization of LD and haplotype maps. Bioinformatics 21:263–265

Blacker D, Bertram L, Saunders AJ, Moscarillo TJ, Albert MS, Wiener H, Perry RT, Collins JS, Harrell LE, Go RC, Mahoney A, Beaty T, Fallin MD, Avramopoulos D, Chase GA, Folstein MF, McInnis MG, Bassett SS, Doheny KJ, Pugh EW, Tanzi RE; NIMH Genetics Initiative Alzheimer's Disease Study Group (2003) Results of a high-resolution genome screen of 437 Alzheimer's disease families. Hum Mol Genet 12:23–32

Chyung JH, Selkoe DJ (2003) Inhibition of receptor-mediated endocytosis demonstrates generation of amyloid β-protein at the cell surface. J Biol Chem 278:51035–51043

Corder EH, Saunders AM, Strittmatter WJ, Schmechel DE, Gaskell PC, Small GW, Roses AD, Haines JL, Pericak-Vance MA (1993) Gene dose of apolipoprotein E type 4 allele and the risk of Alzheimer's disease in late onset families. Science 261:921–923

Farrer LA, Cupples LA, Haines JL, Hyman B, Kukull WA, Mayeux R, Myers RH, Pericak-Vance MA, Risch N, van Duijn CM (1997) Effects of age, sex, and ethnicity on the association between apolipoprotein E genotype and Alzheimer disease. A meta-analysis. APOE and Alzheimer disease meta analysis consortium. JAMA 278:1349–1356

Fukumori A, Okochi M, Tagami S, Jiang J, Itoh N, Nakayama T, Yanagida K, Ishizuka-Katsura Y, Morihara T, Kamino K, Tanaka T, Kudo T, Tanii H, Ikuta A, Haass C, Takeda M (2006) Presenilin-dependent gamma-secretase on plasma membrane and endosomes is functionally distinct. Biochemistry 45:4907–4914

Gabriel SB, Schaffner SF, Nguyen H, Moore JM, Roy J, Blumenstiel B, Higgins J, DeFelice M, Lochner A, Faggart M, Liu-Cordero SN, Rotimi C, Adeyemo A, Cooper R, Ward R, Lander ES, Daly MJ, Altshuler D (2002) The structure of haplotype blocks in the human genome. Science 296:2225–2229

Gutala RV, Reddy PH (2004) The use of real-time PCR analysis in a gene expression study of Alzheimer's disease post-mortem brains. J Neurosci Methods 132:101–107

Hedrick PW (1987) Gametic disequilibrium measures: proceed with caution. Genetics 117:331–341

Kang DE, Saitoh T, Chen X, Xia Y, Masliah E, Hansen LA, Thomas RG, Thal LJ, Katzman R (1997) Genetic association of the low-density lipoprotein receptor-related protein (LRP), an apolipoprotein E receptor, with late-onset Alzheimer's disease. Neurology 49:56–61

Kelly BL, Vassar R, Ferreira A (2005) β-amyloid-induced dynamin 1 depletion in hippocampal neurons. J Biol Chem 280:31746–31753

Kolsch H, Lutjohann D, Ludwig M, Schulte A, Ptok U, Jessen F, von Bergmann K, Rao ML, Maier W, Heun R (2002) Polymorphism in the cholesterol 24S-hydroxylase gene is associated with Alzheimer's disease. Mol Psychiatry 7:899–902

Kuwano R, Miyashita A, Arai H, Asada T, Imagawa M, Shoji M, Higuchi S, Urakami K, Kakita A, Takahashi H, Tsukie T, Toyabe S, Akazawa K, Kanazawa I, Ihara Y; The Japanese Genetic Study Consortium for Alzheimer's Disease (2006) Dynamin-binding protein gene on chromosome 10q is associated with late-onset Alzheimer's disease. Hum Mol Genet 15:2170–2182

McKhann G., Drachman D, Folstein M, Katzman R, Price D, Stadlan EM (1984) Clinical diagnosis of Alzheimer's disease; report of the NINCDS-ADRDA work group under the auspices of department of health and human services task force on Alzheimer's disease. Neurology 34:939–944

Nyholt DR (2004) A simple correction for multiple testing for SNPs in linkage disequilibrium with each other. Am J Hum Genet 74:765–769

Obar RA, Collins CA, Hammarback JA, Shpetner HS, Vallee RB (1990) Molecular cloning of the microtubule-associated mechanochemical enzyme dynamin reveals homology with a new family of GTP-binding proteins. Nature 347:256–261

Pericak-Vance MA, Bass MP, Yamaoka LH, Gaskell PC, Scott WK, Terwedow HA, Menold MM, Conneally PM, Small GW, Vance JM, Saunders AM, Roses AD, Haines JL (1997) Complete genomic screen in late-onset familial Alzheimer disease. Evidence for a new locus on chromosome 12. JAMA 278:1237–1241

Praefcke GJ, McMahon HT (2004) The dynamin superfamily: universal membrane tubulation and fission molecules? Nat Rev Mol Cell Biol 5:133–147

Sambrook J, Fritsch EF, Maniatis T (1989) Molecular cloning: a laboratory manual. 2nd edn. Cold Spring Harbor Laboratory Press, New York, pp 9.14–9.19

Selkoe DJ (2002) Alzheimer's disease is a synaptic failure. Science 298:789–791